

The Globular Cluster System of NGC 4636 and Formation of Globular Clusters in Giant Elliptical Galaxies*

Hong Soo Park¹, Myung Gyoon Lee¹, Ho Seong Hwang², Sang Chul Kim³, Nobuo Arimoto⁴, Yoshihiko Yamada⁴, Naoyuki Tamura^{5,6}, and Masato Onodera⁷

hspark@astro.snu.ac.kr, mglee@astro.snu.ac.kr, hhwang@cfa.harvard.edu, sckim@kasi.re.kr, arimoto.n@nao.ac.jp, yoshihiko.yamada@nao.ac.jp, naoyuki.tamura@ipmu.jp, and monodera@phys.ethz.ch

ABSTRACT

We present a spectroscopic analysis of the metallicities, ages, and alpha-elements of the globular clusters (GCs) in the giant elliptical galaxy (gE) NGC 4636 in the Virgo cluster. Line indices of the GCs are measured from the integrated spectra obtained with Faint Object Camera and Spectrograph (FOCAS) on the Subaru 8.2 m Telescope. We derive $[\text{Fe}/\text{H}]$ values of 59 GCs based on the Brodie & Huchra method, and $[\text{Z}/\text{H}]$, age, and $[\alpha/\text{Fe}]$ values of 33 GCs from the comparison of the Lick line indices with single stellar population models. The metallicity distribution of NGC 4636 GCs shows a hint of a bimodality with two peaks at $[\text{Fe}/\text{H}] = -1.23(\sigma = 0.32)$ and $-0.35(\sigma = 0.19)$. The age spread is large from 2 Gyr to 15 Gyr and the fraction of young GCs with age < 5 Gyr is about 27%. The $[\alpha/\text{Fe}]$ of the GCs shows a broad distribution with a mean value $[\alpha/\text{Fe}] \approx 0.14$ dex. The dependence of these chemical properties on the galactocentric radius is weak. We also derive the metallicities, ages, and $[\alpha/\text{Fe}]$ values

¹Astronomy Program, Department of Physics and Astronomy, Seoul National University, Korea

²Smithsonian Astrophysical Observatory, 60 Garden Street, Cambridge, MA 02138, USA

³Korea Astronomy and Space Science Institute, Daejeon 305-348, Korea

⁴National Astronomical Observatory of Japan, Tokyo, Japan

⁵Kavli Institute for Physics and Mathematics of the Universe, University of Tokyo, Kashiwa-city 277-8583, Japan

⁶Subaru Telescope, National Astronomical Observatory of Japan, Hilo, USA

⁷Institute for Astronomy, ETH Zürich, Wolfgang-Pauli-strasse 27, 8093 Zürich, Switzerland

*Based on data collected at Subaru Telescope, which is operated by the National Astronomical Observatory of Japan.

for the GCs in other nearby gEs (M87, M49, M60, NGC 5128, NGC 1399, and NGC 1407) from the line index data in the literature using the same methods as used for NGC 4636 GCs. The metallicity distribution of GCs in the combined sample of seven gEs including NGC 4636 is found to be bimodal, supported by the KMM test with a significance level of $>99.9\%$. All these gEs harbor some young GCs with ages less than 5 Gyr. The mean age of the metal-rich GCs ($[\text{Fe}/\text{H}] > -0.9$) is about 3 Gyr younger than that of the metal-poor GCs. The mean value of $[\alpha/\text{Fe}]$ of the gE GCs is smaller than that of the Milky Way GCs. We discuss these results in the context of GC formation in gEs.

Subject headings: galaxies: abundances — galaxies: elliptical and lenticular, cD — galaxies: individual (NGC 4636, M87, M49, M60, NGC 5128, NGC 1399, NGC 1407) — galaxies: star clusters: general

1. Introduction

It is generally believed that the stars in a globular cluster (GC) are born almost at the same time and have similar metal abundances, even though there are some GCs with multiple stellar populations in the Milky Way (MW) (Marino et al. 2009; Lee et al. 2009; Bellini et al. 2010). GCs are often assumed as single stellar population (SSP) systems and their observed quantities can be compared with theoretical models for the estimation of their physical parameters. They also contain information on the formation and evolution of their host galaxies. Therefore, analysis of their ages and metallicities can provide critical clues for understanding the evolution of their host galaxies.

According to the current models of structure formation, giant elliptical galaxies (gEs) are considered to form and evolve through mergers with various galaxies. They might have accreted thousands of GCs and sometimes formed new star clusters during the merging process (Lee 2003; Brodie & Strader 2006; Lee et al. 2010a). Therefore, investigation of ages and metallicities of the GCs in gEs may allow us to understand how GCs and their host galaxies formed and evolved. Though, in the case of gEs, it is not possible to obtain detailed information on the resolved stars in GCs with current telescopes, we can effectively estimate their age and metallicity using integrated spectroscopy.

There are several studies on the ages and metallicities of GCs in nearby gEs based on integrated spectroscopy, which are summarized briefly below for six gEs (NGC 5128, M87, M49, M60, NGC 1407, NGC 1399). Basic properties of these galaxies are given in Table 3 of Lee et al. (2010a).

The GCs of the nearest gE NGC 5128 were extensively studied thanks to its relatively short distance, 3.8 Mpc (Peng et al. 2004; Beasley et al. 2008; Woodley et al. 2010; Woodley & Gómez 2010). Recently, Woodley et al. (2010) derived the metallicities, ages and $[\alpha/\text{Fe}]$ values for 72 GCs in NGC 5128 using the Lick indices obtained with the Gemini/GMOS. Ninety-two percent of the metal-poor GCs (MP GCs) have ages older than 8 Gyr, while 56 percent of the metal-rich GCs (MR GCs) do so. They found that the metallicity distribution of the NGC 5128 GCs is bimodal if seen through the metallicities derived directly from the spectroscopic Lick indices ($[\text{MgFe}]'$), but the distribution is not well constrained if they use Lick indices and SSP models. From these results together with the $[\alpha/\text{Fe}]$ data, they suggested that most GCs in NGC 5128 formed rapidly at early times, while some GCs formed later with subsequent major accretion.

The GCs of M87 (NGC 4486), a cD galaxy located at the center of the Virgo cluster, were studied spectroscopically early by Cohen et al. (1998). They reported that the mean metallicity of the GCs is higher than that of the MW GCs, and that the metallicity distribution shows a bimodal feature with peaks at $[\text{Fe}/\text{H}] = -1.3$ and -0.7 . The metallicities of the M87 GCs show a small radial gradient with a large scatter, but the ages of the GCs show no radial gradient. They suggested that the median age of the M87 GCs is 13 Gyr, similar to that of the MW GCs.

M49 (NGC 4472) is the brightest gE in the Virgo cluster. Cohen et al. (2003) presented the spectroscopic results of 47 GCs in this galaxy obtained with the Keck telescope. They concluded that the M49 GCs have slightly higher metallicities than the M87 GCs, while other metallicity and age parameters are basically similar to those of the M87 GCs. They estimated that the mean age of these GCs is about 10 Gyr.

Pierce et al. (2006) reported a study of 38 GCs in M60 (NGC 4649) in the Virgo cluster. They found that several young (2 – 3 Gyr old) GCs in this galaxy have supersolar metallicities, while the majority of the GCs have a wide range of metallicity ($[\text{Fe}/\text{H}] = -2.0$ to 0.0), and are older than 10 Gyr. They also found that the alpha-element ratios of the M60 GCs decrease with increasing metallicity.

The GCs in NGC 1407, the brightest galaxy in the NGC 1407 subgroup of the Eridanus group, were studied recently by Cenarro et al. (2007). They found that 20 GCs are mostly old, while three GCs could be young (~ 4 Gyr). The metallicity of the GCs reaches up to slightly above solar and the mean $[\alpha/\text{Fe}]$ ratio is ~ 0.3 dex, similar to that of the MW GCs.

Spectroscopic properties of the GCs in NGC 1399, gE in the center of the Fornax cluster, were studied early by Kissler-Patig et al. (1998) and Forbes et al. (2001). From the Keck spectra of 10 GCs, Forbes et al. (2001) showed that at least some of the GCs have supersolar

metal abundances. Two GCs with significantly higher $H\beta$ values and enhanced abundance ratios could be regarded as young (~ 2 Gyr) or extremely old (~ 15 Gyr) ages with a warm blue horizontal branch. From this they proposed a possibility of a complicated age distribution among the MR GCs and of some constraints on their chemical enrichment at later epochs.

These previous studies have some limitations. The number of the studied galaxies in this regard is only six, and the number of GCs in each galaxy is still small. The areal coverage for some galaxies is not wide enough, either. Therefore, it is needed to obtain new spectroscopic data for more GCs in each galaxy and for more gEs in order to better understand the chemical properties of gE GCs.

We carried out a spectroscopic study of GCs in another Virgo gE NGC 4636. NGC 4636, located at the southeast boundary of the Virgo, harbors GC populations with a wide spatial distribution (Lee et al. 2010b). It is one of the best targets for the study of age and metal abundance using the integrated spectroscopy together with M87, M49, and M60. There are several previous studies on the photometry, kinematics, and X-ray imaging of NGC 4636 GCs (summarized below), but there is no published study of the metallicities, ages, and alpha-elements for the GCs based on spectroscopy.

The specific frequency of NGC 4636 GCs is $S_N = 5.6 - 8.9$, larger than those of other elliptical galaxies in the Virgo Cluster (Kissler et al. 1994; Dirsch et al. 2005). The GCs of NGC 4636 show a bimodal color distribution, while brighter GCs have intermediate colors (Dirsch et al. 2005). The number of blue GCs is larger than that of red GCs. The number of the red GCs connected with low-mass X-ray binaries is about two times larger than that of the blue GCs (Kim et al. 2006; Posson-Brown et al. 2009).

Using the radial velocity data for NGC 4636 GCs, Schuberth et al. (2006) reported that the dark matter fraction within one effective radius is $20\% \sim 30\%$. However, Chakrabarty & Raychaudhury (2008) suggested that the dark matter distribution is highly concentrated toward the inner halo. Lee et al. (2010a) also confirmed the need of a large amount of dark matter. Schuberth et al. (2006) and Lee et al. (2010a) found that the velocity dispersion for the blue GCs is slightly larger than that for the red GCs. They also studied the radial variation, the rotation, and the orbit of NGC 4636 GC sub-populations.

We have been carrying out a project to investigate the spectroscopic properties of the GCs in nearby galaxies to understand the formation of GCs in galaxies. Our study on the kinematics of the GC system of M60 was presented in Lee et al. (2008b) and Hwang et al. (2008), and another on the GC system of the spiral galaxy M31 was given in Kim et al. (2007) and Lee et al. (2008c). Recently, we presented the measurement of radial velocities

for the GCs in NGC 4636 in a companion paper (Park et al. 2010), and detailed kinematic analysis of these data in Lee et al. (2010a). We also presented a spectroscopic study of the M86 GCs (Park et al. 2012b). Here we present the chemical analysis of the NGC 4636 GCs. By combining the GC data of seven gEs (including NGC 4636) available in the literature, we also investigate the chemical properties of the gE GCs.

This paper is composed as follows. Section 2 describes briefly the spectroscopic observation and data reduction. In §3 we explain how we determine metallicities, ages, and alpha-elements of the GCs using the line indices measured in the optical spectra. §4 presents the chemical analysis results of NGC 4636 GCs. In §5, we compare the chemical properties of NGC 4636 GCs with those of other gEs, and discuss the implication of the results. Primary results are summarized in §6.

2. Observation and Data Reduction

We carried out a spectroscopic observation of GCs in NGC 4636, using the Faint Object Camera and Spectrograph (FOCAS; Kashikawa et al. 2002) at the Subaru 8.2 m Telescope. The spectra were obtained in Multi-Object Spectrography (MOS) mode of FOCAS. Target selection, spectroscopic observation, data reduction, and velocity measurement were described in detail in Park et al. (2010). We obtained flux-calibrated spectra of the targets using BD+33d2642, a standard star for flux calibration taken together with the targets. For the calibration of line indices, we used the spectra of five MW GCs (M5, M13, M92, M107, and NGC 6624) observed in the long slit mode during the same observing run.

In Figure 1, we show the flux-calibrated spectra of an MR GC and an MP GC in NGC 4636, NGC 6624 and M13 in the MW Galaxy, and the NGC 4636 nucleus. These spectra are normalized at about 5400 Å. These spectra show strong absorption lines typically seen in GCs such as $H\beta$, Mgb, and FeI. MR GCs (Figure 1 (a) and (d)) have strong absorption lines at Mgb, while MP GCs (Figure 1 (b) and (e)) have relatively weak lines. Note that there are some sky-line residuals at ~ 5577 Å, which are less than 2% of their original sky-lines. Although these residuals remain because of incomplete distortion correction in the optics, they affect little the index analysis in this study.

3. Metallicity, Age, and $[\alpha/\text{Fe}]$ Measurement

3.1. Line index measurement

We measured two kinds of absorption line indices from the spectra of NGC 4636 GCs: (1) the Brodie & Huchra (1990) line indices, used for determining the metallicities of GCs with empirical relations between absorption line indices and metallicities, and (2) the Lick line indices, used for measuring the metallicities, ages, and alpha-elements from the comparison with SSP models. Following subsections describe the measurement of each index.

3.1.1. Brodie & Huchra (BH) line indices

Brodie & Huchra (1990) and Huchra et al. (1996) presented linear relations between absorption line strength indices obtained from the integrated spectra of old stellar systems and their mean metallicity to determine the metal abundance of the systems. Their method was developed to minimize the systematic effects such as reddening, individual element abundance anomalies, and instrumental effects. They used the spectra and infrared colors of the MW GCs, M31 GCs, and NGC 188 giant stars for the metallicity calibration of the observed spectra.

We measured the absorption line indices from the flux-calibrated spectra of NGC 4636 GCs after shifting each spectrum to the rest frame following the prescription of Brodie & Huchra (1990) and Huchra et al. (1996). The measured absorption line indices are calibrated to the BH index system with a zero point offset, $Index(\text{BH}) = Index(\text{Subaru}) + constant$, determined from the spectra of five MW GCs common in this study and Huchra et al. (1996). The offsets (the *constant* in the above equation) we derived are 0.014 ± 0.015 for G band, -0.013 ± 0.009 for MgH, -0.021 ± 0.018 for Mg2, and 0.008 ± 0.009 for Fe5270. Among the 105 NGC 4636 GCs with measured velocities (Park et al. 2010), we derived the BH line indices for 59 GCs with $S/N \gtrsim 10$ and $T_1 < 21$. The resulting index errors are smaller than 0.10 mag for G band, 0.03 mag for MgH and Mg2, and 0.04 mag for Fe5270.

3.1.2. Lick line indices

Lick absorption line indices are useful for measuring the metallicity and age of old stellar systems from the integrated spectra with low/medium resolution (Puzia et al. 2002, 2005a; Beasley et al. 2008; Trager et al. 2008; Woodley et al. 2010). We measured the Lick line indices as follows. We first smoothed our spectra with the Lick resolution (Worthey & Ottaviani

1997) after shifting each spectrum to the rest frame. Then we derived the Lick line indices from the spectra of NGC 4636 GCs, following the definitions and the methods given in Worthey (1994) and Worthey & Ottaviani (1997). Line index errors are derived from the photon noise in the spectra before the flux calibration. Then we calibrated the resulting line indices to the Lick system with the zero point offset, $Index(\text{Lick}) = Index(\text{Subaru}) + constant$, determined from the spectra of five MW GCs common in this study, Trager et al. (1998), and Kuntschner et al. (2002).

Table 1 lists the zero point offsets derived in this study. The first, second, third, and fourth column are the name of the Lick index, unit of each index, zero point offset, and *rms*, respectively. Note that these offsets are slightly different from those in Paudel et al. (2010); these differences could systemically lead to the uncertainties of 2.3 Gyr in age, 0.14 dex in metallicity, and 0.18 dex in alpha-elements. We finally measure the Lick line indices for 33 GCs in NGC 4636, listed in Tables 2 and 3. The associated errors are in Tables 4 and 5. We use only the spectra with $S/N \gtrsim 15$, where the S/N value is measured at the continuum part of the Lick line indices such as $H\beta$, Mg_2 , Mgb , $Fe5270$, and $Fe5335$.

3.2. Determination of Metallicity, Age, and $[\alpha/Fe]$

We derived metallicity using three methods (the Brodie & Huchra method, the Lick index grid method and the χ^2 minimization method), and age and $[\alpha/Fe]$ using two methods (the Lick index grid method and the χ^2 minimization method) for NGC 4636 GCs. Each method is described below.

3.2.1. Brodie & Huchra (BH) method

We use the method described in Brodie & Huchra (1990) to derive metallicities from the absorption line indices for NGC 4636 GCs. They recommended six best indices (G band, MgH , Mg_2 , $Fe5270$, CNB, and Δ) as the primary calibrators among the 12 line indices for the empirical relations between the BH line indices and the metallicities. We used, however, only four primary line indices to determine the metallicities of NGC 4636 GCs, excluding CNB and Δ because of low S/N values in their wavelength range. The relations between metallicity and the four indices are as follows. $[Fe/H]_{Gband} = 11.415 \times Gband - 2.455$, $[Fe/H]_{MgH} = 20.578 \times MgH - 1.840$, $[Fe/H]_{Mg_2} = 9.921 \times Mg_2 - 2.212$, and $[Fe/H]_{Fe5270} = 20.367 \times Fe5270 - 2.086$. We then derive the final metallicity value of each GC by taking an error-weighted average of four measurements. Here the error is the mean of the standard

deviation. The mean error for 59 GCs derived from this method is 0.31 ± 0.16 dex with the maximum error of about 0.6 dex.

3.2.2. Lick index grid method

To obtain the estimates of metallicity, age, and $[\alpha/\text{Fe}]$ from the integrated spectra of the NGC 4636 GCs, we use the Lick index grid method (the grid method hereafter), which is to derive the age and abundance from the comparison of the Lick indices with the line index grids predicted from SSP models (Tripicco & Bell 1995; Trager et al. 2000; Thomas et al. 2004; Puzia et al. 2005a). Here, we adopt SSP models given by Thomas et al. (2003, 2004, 2005).

We use the grids of $[\text{MgFe}]'$ versus $\text{H}\beta$ provided by Thomas et al. (2003) to estimate the metallicity and age of each GC. The composite index $[\text{MgFe}]'$, defined as $[\text{MgFe}]' = \sqrt{\text{Mgb} \times (0.72 \times \text{Fe5270} + 0.28 \times \text{Fe5335})}$, is a good tracer of metallicity because of little sensitivity to $[\alpha/\text{Fe}]$ (Thomas et al. 2003). We use $\text{H}\beta$ as an age indicator, which is the least sensitive to $[\alpha/\text{Fe}]$ among the Balmer lines (Thomas et al. 2003). We also use the grids of Mg_2 versus $\langle\text{Fe}\rangle$ in order to derive $[\alpha/\text{Fe}]$ estimates. The Mg_2 index is very sensitive to $[\alpha/\text{Fe}]$, and the $\langle\text{Fe}\rangle$ index, defined as $\langle\text{Fe}\rangle = (\text{Fe5270} + \text{Fe5335})/2$, is a metallicity indicator on this grid (Thomas et al. 2003).

Figure 2 shows the measured indices in comparison with SSP model grids for various values of $[\text{Z}/\text{H}]$ and age. Panel (a) displays the Lick line indices of $\text{H}\beta$ versus $[\text{MgFe}]'$ for the NGC 4636 GCs measured in this study as well as those for the NGC 5128 GCs (Woodley et al. 2010) for comparison. Grids indicate several values of $[\text{Z}/\text{H}]$ (-2.25 , -1.35 , -0.33 , 0.0 , 0.35 , and 0.67 dex) and ages (0.4, 0.6, 0.8, 1, 2, 3, 5, 8, 10, and 15 Gyr) from the SSP model with $[\alpha/\text{Fe}] = 0.2$. The NGC 4636 GCs show a large dispersion in ages; most of them are old and some GCs are younger than 5 Gyr. The GCs in NGC 4636 and in NGC 5128 show similar age distributions, while the latter have a relatively small number of young GCs than the former. Metallicities of GCs in NGC 4636 and in NGC 5128 show a wide dispersion at $[\text{Z}/\text{H}] < 0.7$ dex. Panel (b) displays $\langle\text{Fe}\rangle$ versus Mg_2 , with the SSP grids for age = 8 Gyr (mean age of our sample). While the scatter looks large, most GCs in NGC 4636 are concentrated on $[\alpha/\text{Fe}]$ of ~ 0 and ~ 0.5 . GCs in NGC 5128 also show a large dispersion and most of them are located at $[\alpha/\text{Fe}] \sim 0$. In the followings, quantitative analyses on the age, metallicity, and $[\alpha/\text{Fe}]$ of NGC 4636 GCs are shown.

Since the dependence of the $\text{H}\beta$ versus $[\text{MgFe}]'$ grid on $[\alpha/\text{Fe}]$ is not negligible, we need $[\alpha/\text{Fe}]$ information for accurate estimation of age and metallicity. An Mg_2 versus $\langle\text{Fe}\rangle$ grid

also needs an age value for accurate estimation of $[\alpha/\text{Fe}]$ and metallicity. Thus we need an iteration between the two grids in order to determine age, metallicity, and $[\alpha/\text{Fe}]$ of an object more accurately. We follow the iteration technique described in Puzia et al. (2005a), which is summarized in the following. First, the age and metallicity of one GC is determined from the $\text{H}\beta$ versus $[\text{MgFe}]'$ grid in a given $[\alpha/\text{Fe}]$ as in Figure 2 (a). Next, we determine the $[\alpha/\text{Fe}]$ and metallicity using the $\langle\text{Fe}\rangle$ versus Mg_2 grid with a previously determined age as in Figure 2 (b). Then, we derive again the age and metallicity of the GC using the $\text{H}\beta$ versus $[\text{MgFe}]'$ grid at the $[\alpha/\text{Fe}]$ value obtained above. We repeat this iteration until the $[\text{Z}/\text{H}]$ difference converges to smaller than 0.01 dex. Finally, the converged values are selected as final values of age, metallicity, and $[\alpha/\text{Fe}]$ of the GC.

To estimate the errors of the age, metallicity, and $[\alpha/\text{Fe}]$ values of a GC, we calculate ages, metallicities, and $[\alpha/\text{Fe}]$ values of the four data points composed of $\text{H}\beta \pm$ error and $[\text{MgFe}]' \pm$ error in the $\text{H}\beta$ versus $[\text{MgFe}]'$ grid and $\langle\text{Fe}\rangle \pm$ error and $\text{Mg}_2 \pm$ error in the $\langle\text{Fe}\rangle$ versus Mg_2 grid. The difference between the average of these four values and the estimate directly calculated from the *index* is taken as the final error for the age, metallicity, and $[\alpha/\text{Fe}]$ of the GC. For some GCs outside the model grid, we adopt the value of the nearest envelope of the model grid in the direction of error vector as their estimates following Puzia et al. (2005a). For example, if the data points are below the grid limit in the $\text{H}\beta$ versus $[\text{MgFe}]'$ diagram, we adopt the maximum value of age (i.e. 15 Gyr) at $[\text{Z}/\text{H}] > -0.5$ dex, but the age value of about 12 Gyr due to some overlapped grids at $[\text{Z}/\text{H}] < -0.5$ dex. For the data points below the grid limit in the $\langle\text{Fe}\rangle$ versus Mg_2 diagram, we also adopt the maximum value of $[\alpha/\text{Fe}]$ (i.e. 0.5 dex).

3.2.3. χ^2 minimization method

Proctor et al. (2004) suggested a method that can measure the physical parameters (metallicity, age, and alpha-elements) for GCs in a robust way based on simultaneous fitting of all the available Lick line indices with χ^2 minimization. We call this method the χ^2 minimization method hereafter. This method maximizes the use of available information, while the grid method uses only a pair of indices. Recently this method was used in the studies of the GCs in gE M60 by Pierce et al. (2006) and early-type dwarf galaxies in Virgo by Paudel et al. (2010).

We applied this method to the NGC 4636 GCs using the same SSP models as used in the grid method. Among 10 Lick line indices except Mg_1 at $4500 - 5750 \text{ \AA}$, we used about eight indices after $\sim 2\sigma$ clipping of their χ . The error of each parameter is the value where χ^2 difference above the minimum reaches 1σ significance level. We list the measured

metallicities, ages, and $[\alpha/\text{Fe}]$ for the NGC 4636 GCs in Table 6.

4. Results

4.1. A Catalog of Metallicity, Age, and $[\alpha/\text{Fe}]$

Among the 105 GCs whose radial velocities are measured in Park et al. (2010), we obtained $[\text{Z}/\text{H}]$, age, and $[\alpha/\text{Fe}]$ for 33 GCs with the grid method and χ^2 minimization method, while we obtained $[\text{Fe}/\text{H}]$ for 59 GCs with the BH method. Table 6 lists metallicities, ages, and $[\alpha/\text{Fe}]$ values for the NGC 4636 GCs.

Figure 3 shows a comparison of the results for NGC 4636 GCs derived from three methods. Panel (a) shows a comparison of the metallicities obtained from the BH method and the grid method. $[\text{Fe}/\text{H}](\text{grid or } \chi^2)$ is converted from the total metallicity, $[\text{Z}/\text{H}]$, using the correlation between the two: $[\text{Fe}/\text{H}] = [\text{Z}/\text{H}] - 0.94 [\alpha/\text{Fe}]$ (Thomas et al. 2003). Here we adopt $[\alpha/\text{Fe}] = 0.2$, which is the mean $[\alpha/\text{Fe}]$ for NGC 4636 GCs. Panel (a) shows a good agreement between the two measurements. We derive a linear least-squares fit: $[\text{Fe}/\text{H}](\text{BH}) = 0.935(\pm 0.080)[\text{Fe}/\text{H}](\text{grid}) + 0.170(\pm 0.069)$ with $rms = 0.227$. In the metal poor region, however, the metallicities derived from the grid method for three GCs are smaller than those from the BH method. Panel (b) illustrates a comparison of the metallicities obtained from the BH method and the χ^2 minimization method, showing a good agreement between the two measurements. We derive a linear least-squares fit: $[\text{Fe}/\text{H}](\text{BH}) = 0.988(\pm 0.072)[\text{Fe}/\text{H}](\chi^2) - 0.105(\pm 0.078)$ with $rms = 0.297$.

Panel (c) displays a relation between $[\text{Z}/\text{H}]$ derived from the $\text{H}\beta$ versus $[\text{MgFe}]'$ grid and that from the $\langle \text{Fe} \rangle$ versus Mg_2 grid. It also shows a good agreement between the two estimates except for three outliers. We derive a linear least-squares fit: $[\text{Z}/\text{H}](\text{Mg}_2) = 0.914(\pm 0.058)[\text{Z}/\text{H}](\text{MgFe}') + 0.105(\pm 0.031)$ with $rms = 0.192$. For the following analysis, we mainly use the metallicities of GCs measured from the $\text{H}\beta$ versus $[\text{MgFe}]'$ grid because the main concerns in this study are the ages rather than the alpha-elements of GCs.

Panel (d) illustrates a comparison of the metallicities obtained from the grid method and the χ^2 minimization method, which shows a good agreement between the two measurements. We derive a linear least-squares fit: $[\text{Z}/\text{H}](\chi^2) = 0.946(\pm 0.073)[\text{Z}/\text{H}](\text{grid}) - 0.092(\pm 0.052)$ with $rms = 0.209$. Panel (e) shows a comparison of the ages obtained from the grid method and the χ^2 minimization method. Panel (e) shows a reasonable agreement between the two measurements with a large scatter. We derive a linear least-squares fit: $\text{Age}(\chi^2) = 1.017(\pm 0.085)\text{Age}(\text{grid}) + 0.057(\pm 0.739)$ with $rms = 2.942$. Note that there are six GCs with ages younger than 5 Gyr derived from both methods. The five out of six GCs have

relatively higher S/N (> 20). Therefore, the existence of young GCs is not simply due to the low S/N spectra (see next section for detailed discussion). Panel (f) shows a comparison of the $[\alpha/\text{Fe}]$ obtained from the grid method and the χ^2 minimization method. It shows a reasonable agreement between the two measurements with a large scatter. We derive a linear least-squares fit: $[\alpha/\text{Fe}] (\chi^2) = 0.934(\pm 0.064)[\alpha/\text{Fe}] (\text{grid}) - 0.042(\pm 0.028)$ with $rms = 0.125$.

4.2. Distributions of Metallicity, Age and $[\alpha/\text{Fe}]$

Figure 4 represents the distributions of metallicity, age, and $[\alpha/\text{Fe}]$ for the GCs in NGC 4636 derived from the three methods. Panel (a) shows that the $[\text{Fe}/\text{H}]$ obtained from the BH method has a wide distribution at $-2.2 < [\text{Fe}/\text{H}] < 0.4$ with the mean value of $[\text{Fe}/\text{H}] = -0.90 \pm 0.12$. Two peaks appear to be at $[\text{Fe}/\text{H}] \sim -1.5$ and ~ -0.4 . The $[\text{Z}/\text{H}]$ distribution obtained from the $[\text{MgFe}]'$ grid method (Figure 4 (b)) shows a similar wide range of $-2.4 < [\text{Z}/\text{H}] < 0.8$ with the mean value of -0.58 ± 0.75 . Two peaks are seen at -1.0 and -0.2 . The results from the χ^2 minimization method (dot-dashed line) are similar to those from the grid method (solid line).

We performed the KMM test to analyze quantitatively the bimodality of the metallicity distribution of NGC 4636 GCs. The KMM test based on the algorithm of Ashman et al. (1994) gives an estimate of the improvement of the n -group fit over a single Gaussian. In our sample, the hypothesis of a unimodal metallicity distribution can be rejected at the 97.1%, 71.4%, 98.4%, and 95.2% confidence level in the case of the $[\text{Fe}/\text{H}]$ obtained from the BH method, the $[\text{MgFe}]'$ grid, the color-metallicity relation, and the χ^2 minimization method, respectively (see Figure 5). These suggest that the metallicity distribution of NGC 4636 GCs is marginally bimodal.

Figure 5 represents the metallicity distributions and their Gaussian fits determined from the KMM test. Panel (a) shows that two peaks are at $[\text{Fe}/\text{H}] = -1.23(\sigma = 0.32)$, and $-0.35(\sigma = 0.19)$. The distribution of $[\text{Fe}/\text{H}]$ determined with $[\text{MgFe}]'$ grid (panel (b)) shows two peaks at $[\text{Fe}/\text{H}] = -1.14(\sigma = 0.22)$ and $-0.41(\sigma = 0.21)$. The distribution of $[\text{Fe}/\text{H}]$ from the χ^2 minimization method (panel (d)) also shows two peaks at $[\text{Fe}/\text{H}] = -1.22(\sigma = 0.25)$ and $-0.44(\sigma = 0.16)$. In addition we derived the photometric metallicity distribution from the $(C - T_1)_0$ color (Park et al. 2012a) using the double linear equation given in Lee et al. (2008a) (panel (c)). It shows two peaks at $[\text{Fe}/\text{H}] = -1.35(\sigma = 0.16)$ and $-0.59(\sigma = 0.28)$. We also plot the metallicity distribution of the MW GCs from Harris (1996) (2010 version) in panel (a) for comparison. It also shows two peaks at $[\text{Fe}/\text{H}] = -1.52(\sigma = 0.39)$ and $-0.52(\sigma = 0.23)$, each of which is at slightly lower values than the

NGC 4636 GCs.

Figure 4 (c) shows that the age distribution of the NGC 4636 GCs has a wide range from young (2 Gyr) to old (15 Gyr) with the mean grid age of 7.9 ± 0.8 Gyr and the mean χ^2 fit age of 8.7 ± 2.0 Gyr. The results from both methods are similar. It seems that there are three peaks at 3, 8, and 14 Gyr. If we divide the age distribution into three bins of $t < 5$ Gyr, $5 < t < 10$ Gyr, and $t > 10$ Gyr, the number ratios are 9:13:11 (27:39:34%) in the grid age and 9:10:14 (27:30:43%) in the χ^2 fit age. The fraction of the young GCs with age < 5 Gyr in our sample is about 27%, which is a slightly larger than that (18%) in NGC 5128 (Woodley et al. 2010).

To check the robustness of the large fraction of young GCs in NGC 4636, we first divide the GCs into two groups based on their S/N: 22 GCs with $S/N > 20$ and 11 GCs with $S/N < 20$. The GCs in the two groups do not show any difference in their age distributions. There are six young (age < 5 Gyrs) GCs among 22 GCs with $S/N > 20$. Similarly, there are three young GCs among 11 GCs with $S/N < 20$. These suggest that the existence of young GCs is not simply because of spectra with low S/N. However, Brodie et al. (2005) argued that young or intermediate GCs may be due to relatively low S/N spectra or to sky subtraction difficulties. We also computed the probability of the existence of young GC with age < 5 Gyr and $S/N > 20$ using a simple simulation with GCs of age = 9 Gyr (a mean age of NGC 4636 GCs) and of Hbeta error = 0.34 A (a mean value of measured errors). The fraction of young GCs with age < 5 Gyr derived from simulations is 12%, which is smaller than the observational fraction (27%). This result indicates that the young GCs in NGC 4636 could be caused in part by observational uncertainty. The reliability of the existence of young GCs needs to be checked with better data in the future.

Alpha-element abundances indicate the duration of star formation in a GC. The GCs with an enhanced $[\alpha/\text{Fe}]$ ratio experienced rapid star formation over less than 1 Gyr timescale, while solar $[\alpha/\text{Fe}]$ GCs have an extended star formation history (Brodie & Strader 2006). Figure 4 (d) displays the distribution of $[\alpha/\text{Fe}]$. The overall distribution in the grid method shows a single peak with a large dispersion except for those at both ends, while that from the χ^2 minimization method does not show a dominant peak. The mean $[\alpha/\text{Fe}]$ is derived to be 0.20 ± 0.11 in the grid method and 0.07 ± 0.05 in the χ^2 minimization method. This mean value is between the values for the NGC 5128 GCs ($[\alpha/\text{Fe}] = 0.13 \pm 0.03$ in the grid method and $[\alpha/\text{Fe}] = 0.06 \pm 0.03$ in the χ^2 minimization method, see Table 10) and for the MW GCs ($[\alpha/\text{Fe}] = 0.36 \pm 0.01$). This suggests that the formation period of NGC 4636 GCs might have been more extended, as in the case of NGC 5128 GCs, than the MW GCs.

4.3. Radial distribution

We investigated the distributions of the metallicity, age, and $[\alpha/\text{Fe}]$ of the NGC 4636 GCs as a function of the galactocentric distance. Figure 6 (a), (b), and (e) show that $[\text{Fe}/\text{H}]$ and $[\text{Z}/\text{H}]$ (from BH, grid, and χ^2 minimization methods) vary little with the galactocentric radii at $R < 8'$ (< 34 kpc), but show a large scatter. It is noted that four GCs at $8' < R < 10'.5$ have on average ~ 0.5 dex lower $[\text{Fe}/\text{H}]$ values than the GCs in the inner region. Figure 6 (c) and (f) show that the mean age of the NGC 4636 GCs changes little with the galactocentric radii and the dispersion in age is large. This trend is similarly found in M60 GCs (Pierce et al. 2006). Panels (d) and (g) show no radial dependence of $[\alpha/\text{Fe}]$.

4.4. Relation between metallicity and age

Figure 7 displays the relations between metallicity and age for the NGC 4636 GCs in comparison with NGC 5128 GCs and the MW GCs. The NGC 4636 GCs show, on average, an anti-correlation between age and metallicity. Younger GCs in NGC 4636 have higher metal abundances in both grid and χ^2 minimization results. It is also seen in the case of NGC 5128 GCs (see also Woodley et al. (2010)) and the MW GCs. This correlation is also seen for the GCs in M60 (Pierce et al. 2006) and M86 (Park et al. 2012b). Note that this correlation could be caused by the correlated errors of age and metallicity (see the error boxes in Figure 7) (Trager et al. 2000; Kuntschner et al. 2001; Paudel et al. 2010) or by a biased sample selection (e.g., extremely bright GCs) (Woodley et al. 2010). The age of the youngest GCs in the MW is 7 Gyr, but NGC 4636 and NGC 5128 have a significant number of GCs younger than 7 Gyr. The relative fraction of old (> 10 Gyr) GCs in NGC 4636 is smaller than that of NGC 5128 GCs and much smaller than that of MW GCs.

5. Discussion

In this study, we derived the metallicity, age, and $[\alpha/\text{Fe}]$ for the GCs in NGC 4636 from the spectroscopic data. Here we compare these with those of GCs in other nearby gEs and discuss the results in the context of GC formation in gEs. We found six gEs for which the spectroscopic data of their GCs are available in the literature. We compiled the Lick line index measurements for the GCs in each galaxy from the following references: Cohen et al. (1998) for M87, Beasley et al. (2000) and Cohen et al. (2003) for M49, Woodley et al. (2010) for NGC 5128, Pierce et al. (2006) for M60, Cenarro et al. (2007) for NGC 1407, and Forbes et al. (2001) for NGC 1399. To have a fair comparison of physical

parameters among gEs, we re-derived the metallicity, age, and $[\alpha/\text{Fe}]$ for the GCs in each gE from the line indices using both grid and χ^2 minimization methods as done for NGC 4636 GCs (see Section 3.2). We also compared the GCs in gEs with the MW GCs. The data of the MW GCs are obtained from Harris (1996) (2010 version) for metallicity, from Marín-Franch et al. (2009) and Dotter et al. (2010) for age, and from Carretta et al. (2010) for $[\alpha/\text{Fe}]$.

5.1. Metallicity distribution of GCs in gEs

The color bimodality in recent extragalactic GC studies is one of the important ingredients for GC formation scenarios (Brodie & Strader 2006). This bimodal color distribution is interpreted as an intrinsic property due to a bimodal metallicity distribution (Brodie & Strader 2006; Spitler et al. 2008; Woodley et al. 2010; Chies-Santos et al. 2012), or an apparent feature simply due to a nonlinear color-metallicity relation (Yoon et al. 2006, 2011a,b). It is not yet clear which of these two is more supported by observational results. Here we investigate the metallicity distributions of the GCs in seven gEs.

Figure 8 displays the distributions of metallicity derived with the grid method for the GCs in seven gEs. The metallicity distributions of GCs in most gEs seem to be bimodal as in the case of the MW GC system (see Figure 5 (a)). We run the KMM test for quantitative analysis of the metallicity distribution, and list the results for the Gaussian peaks and their confidence levels in Table 7. There is no strong evidence for the bimodality for NGC 4636, M60, NGC 1407, and NGC 1399 that have a relatively small number of GCs. However, the bimodality for NGC 5128, M87, and M49 is supported by the KMM test with a confidence level $\gtrsim 98\%$.

We combine the data derived from the grid method for all the GCs in seven gEs, and show the resulting metallicity distribution in Figure 8 (h). The combined gE sample (304 GCs) shows clearly a bimodal distribution (155 MP GCs and 149 MR GCs). The KMM test yields two Gaussian peaks at $[\text{Fe}/\text{H}] = -1.21(\sigma = 0.32)$, and $-0.42(\sigma = 0.27)$ with 99.9% confidence level. The MR peak for the combined gE sample is ~ 0.1 dex higher than that for the MW GCs ($[\text{Fe}/\text{H}] = -0.52(\sigma = 0.23)$), while the MP peak is ~ 0.3 dex higher than that of the MW GCs ($[\text{Fe}/\text{H}] = -1.52(\sigma = 0.39)$). It is noted that there are two more minor components at both ends ($[\text{Fe}/\text{H}] < -2.0$ and $[\text{Fe}/\text{H}] > 0.0$) in the combined gE sample.

Figure 9 displays the distributions of metallicity derived with the χ^2 method for the GCs in seven gEs. The KMM test results for the Gaussian peaks and their confidence levels are given in Table 7. There is no strong evidence for the bimodality only for two

gEs (NGC 1399 and NGC 1407). However, the bimodality for NGC 4636, NGC 5128, M60, M87, and M49 is supported by the KMM test with a confidence level $\geq 95\%$. The combined gE sample (315 GCs) shows clearly a bimodal distribution (167 MP GCs and 148 MR GCs). The KMM test yields two Gaussian peaks at $[\text{Fe}/\text{H}] = -1.25(\sigma = 0.32)$, and $-0.42(\sigma = 0.25)$ with 99.9% confidence level, which are very similar to those from the grid method, $[\text{Fe}/\text{H}] = -1.21(\sigma = 0.32)$, and $-0.42(\sigma = 0.27)$. It is noted that there are two more minor components at both ends ($[\text{Fe}/\text{H}] < -2.0$ and $[\text{Fe}/\text{H}] > 0.0$) in the combined gE sample, as found in the results from the grid method.

To examine any age dependence of the metallicity distribution of the GCs in gEs, we divide the GC samples into two groups: young GCs with age ≤ 10 Gyr and old GCs with age > 10 Gyr. In Figures 8 and 9, we plot the metallicity distribution of the young GCs and old GCs (the dotted and dot-dashed lines, respectively). We also derive the mean metallicities of the young GCs and old GCs, which are marked with the vertical lines in Figures 8 and 9 (see also Table 8). The mean values are determined with the biweight location (Beers et al. 1990), and their errors indicate the 68% confidence levels obtained with a bootstrap method. The mean metallicity of all GCs in gEs ($[\text{Fe}/\text{H}] = -0.80 \pm 0.04$ and -0.86 ± 0.04 from the grid method and the χ^2 minimization method, respectively) is much higher than that for the MW GCs ($[\text{Fe}/\text{H}] = -1.28 \pm 0.05$). The mean metallicity of the young GCs in each gE and the MW is 0.2 – 1.3 dex higher than that of the old GCs. For the combined sample, the mean metallicities of the young GCs and old GCs are $[\text{Fe}/\text{H}] = -0.55 \pm 0.05$ and $[\text{Fe}/\text{H}] = -0.96 \pm 0.05$ in the case of the grid method, and $[\text{Fe}/\text{H}] = -0.65 \pm 0.06$ and $[\text{Fe}/\text{H}] = -1.00 \pm 0.04$ in the case of the χ^2 minimization method. Thus the metallicity of the young GCs is, on average, ~ 0.4 dex higher than that of the old GCs. It is noted that both old and young GCs appear to show a bimodal distribution. However, the MP component is dominant for the old GCs, while the MR component is dominant for the young GCs.

We also examine a relation between metallicity and $[\alpha/\text{Fe}]$. We divide the sample into two groups: high $[\alpha/\text{Fe}] > 0.2$ and low $[\alpha/\text{Fe}] \leq 0.2$. The results are listed in Table 8. The mean metallicity of GCs does not show any significant dependence on $[\alpha/\text{Fe}]$, except for two gEs (NGC 1407 and NGC 1399) with a small number of GCs. Note that some of the differences between galaxies could be dominated by selection effects (e.g., different brightness of GCs) or by small number statistics.

5.2. Age distribution of GCs in gEs

Figures 10 and 11 show the age distributions of the GCs in gEs derived from the grid method and from the χ^2 minimization method, respectively. We also plot the age distribution

of the GCs in the combined sample for gEs (panel (h)). We divide the sample into subgroups according to their metallicity and $[\alpha/\text{Fe}]$: MP groups with $[\text{Fe}/\text{H}] \leq -0.9$ and MR groups with $[\text{Fe}/\text{H}] > -0.9$, and low $[\alpha/\text{Fe}]$ groups with $[\alpha/\text{Fe}] \leq 0.2$ and high $[\alpha/\text{Fe}]$ groups with $[\alpha/\text{Fe}] > 0.2$. We derive the mean ages of each group, which are listed in Table 9. The mean values of the metallicity subgroups are shown by the vertical lines in Figures 10 and 11.

Several features are noted in these figures. First, all gEs in this sample show a wide range of ages for GCs, from 1 Gyr to 15 Gyr. This is in stark contrast to the case of the MW GCs. The MW GCs are all older than 7 Gyr and mostly older than 10 Gyrs (see Figure 7). Second, the mean age for the MP GCs in the combined sample (12.2 ± 0.1 Gyr from both methods) is about 3 Gyr larger than that for the MR GCs (9.2 ± 0.7 Gyr from the grid method and 9.7 ± 0.7 Gyr from the χ^2 minimization method, respectively). The MW GCs show similar trends, but with a smaller difference of 1 Gyr: 12.9 ± 0.3 Gyr for the MP GCs, 11.8 ± 0.2 Gyr for the MR GCs. Third, the mean age for the high $[\alpha/\text{Fe}]$ GCs in the combined sample is similar to that for the low $[\alpha/\text{Fe}]$ GCs, while the high $[\alpha/\text{Fe}]$ GCs in the MW are, on average, older than the low $[\alpha/\text{Fe}]$ GCs.

In Figure 12 we plot the mean age and metallicity for all, MP, and MR GCs as a function of absolute magnitude (M_B) of gEs. The mean ages of the GCs (in the upper panels) do not show any systematic dependence on M_B of gEs. The mean ages of the MP GCs show little scatter, while those of the MR GCs show a large scatter. It is noted, however, that two galaxies with low luminosity (NGC 1399 and NGC 4636) have the smallest mean ages of MR GCs. The mean metallicities of the GCs derived from both methods (in the lower panels) also show little dependence on the absolute magnitudes of their host galaxies. Note that the results for all GCs and old GCs in gEs are not consistent with the results derived from photometry of GCs for early-type galaxies in Virgo by Peng et al. (2006) (dashed lines), while those for young GCs are. Further studies are needed to explain this difference.

5.3. $[\alpha/\text{Fe}]$ distribution of GCs in gEs

Figure 13 shows the $[\alpha/\text{Fe}]$ distributions of the GCs in gEs. We also plot the $[\alpha/\text{Fe}]$ distribution of the GCs in the combined sample for gEs and the MW GCs in panel (h). Here we exclude the $[\alpha/\text{Fe}]$ values of M87 GCs in the combined sample from the grid method because of abnormal value of Mg_2 Lick indices in the literature. We divide the sample into subgroups according to their metallicity and age as done in the previous sections. We derive the mean $[\alpha/\text{Fe}]$ of each group, which are listed in Table 10. Notable features are as follows. First, the mean value of $[\alpha/\text{Fe}]$ for the gE GCs ($[\alpha/\text{Fe}] = 0.14 \pm 0.02$ and 0.16 ± 0.01 from the grid method and the χ^2 minimization method, respectively) is about 0.2 dex smaller than that

for the MW GCs, $[\alpha/\text{Fe}] = 0.36 \pm 0.01$. Second, the mean values of $[\alpha/\text{Fe}]$ for the MP and MR GCs in gEs are similar. Third, the mean values of $[\alpha/\text{Fe}]$ for the young and old GCs in gEs are also similar. The old GCs in the MW have much higher $[\alpha/\text{Fe}]$, 0.35 ± 0.11 than the young GCs $[\alpha/\text{Fe}]$, -0.02 ± 0.02 , although the number of the young GCs is only two.

These $[\alpha/\text{Fe}]$ results of the GCs in gEs appear to be inconsistent with those in seven early-type galaxies given by Puzia et al. (2005b), who reported that the mean $[\alpha/\text{Fe}]$ for these gE GCs is high (0.47 ± 0.06). Puzia et al. (2005a) also found that the MR GCs exhibit lower $[\alpha/\text{Fe}]$ enhancements than the MP GCs, and that $[\alpha/\text{Fe}]$ of GCs is independent from the age of GCs. The low $[\alpha/\text{Fe}]$ for gE GCs in this study seems to be more consistent with the stellar populations in massive elliptical galaxies expected from the dissipative hierarchical merging model (Thomas et al. 1999). The discrepancy between this study and Puzia et al. (2005b) could be caused by the mass difference in their host galaxies because the our sample galaxies are more massive than those of Puzia et al. (2005b).

5.4. Formation of GCs in gEs seen through the metallicities and ages

In Figures 14 and 15 we display the metallicity and age of gE GCs derived from the grid and χ^2 minimization methods: (a) age distributions for all, MP, and MR GCs, (b) metallicity and age relation, and (c) metallicity distributions for all, young, and old GCs. The metallicities for gE GCs show an overall anti-correlation with ages, although there is a large scatter: the mean metallicity for GCs increases as the GCs become young. It is also noted that there are both MP and MR GCs in the old age, while there are only MR GCs in the young age. In Table 11, we derived the mean values of metallicity and age for the MR and MP GCs in the young group (age < 10 Gyr) and old group (age > 10 Gyr) in the combined sample of gEs and the MW. The number ratio of the young group and the old group is 1:3 for the MP GCs, and 1:1 for the MR GCs. In the case of the old group, the mean ages for the MR and MP GCs are about 13 Gyrs, and there is little difference in the mean ages between the MR and MP GCs. It is noted that the mean age for the MR GCs in the MW is about one Gyr younger than that for the MP GCs. In the case of the young group, the mean age for the MR GCs is about 5 Gyr, which is about 2 Gyr younger than that for the MP GCs.

Puzia et al. (2005b) reported an existence of the age-metallicity relation based on the high quality spectra for 17 GCs in seven early-type galaxies. The age-metallicity relation shown for gE GCs as well as for MW GCs is also seen in the studies of the GCs in the Large Magellanic Cloud using the high-resolution spectroscopy (Colucci et al. 2011), and of the GCs in six nearby galaxies using the medium-resolution spectroscopy (Sharina et al. 2010).

Therefore, it would be very interesting to examine whether there is a global age-metallicity relation of GCs from dwarf galaxies to massive galaxies.

Recently, Muratov & Gnedin (2010) presented a semi-analytic model for the origin of the metallicity distribution of GCs using the galaxy merging history from the cosmological simulations coupled with observed scaling relations for the amount and metallicity of cold gas available for the star formation. They predicted that early mergers of small galaxies create exclusively MP GCs, while subsequent mergers with more massive galaxies create both MP and MR GCs. Thus they showed the age-metallicity relation, which is that MR GCs are several Gyr younger than MP GCs. They also expected that the mergers with more massive galaxies like the case of gEs would produce comparable numbers of MR and MP GCs simultaneously. Our results, that the MR GCs in gEs are on average ~ 3 Gyr younger than the MP GCs and the fraction of young MR GCs is non-negligible, seem to be consistent with the model prediction by Muratov & Gnedin (2010). However, our result that there are comparable amounts of old MR GCs in gEs is not consistent with their model prediction that exclusively old MP GCs formed in the early stage.

Yoon et al. (2011b) suggested nonlinear color-metallicity relations between the colors of GCs and their metallicities. The shape of the metallicity distribution function (MDF) for GCs, characterized by a sharp peak with a metal-poor tail, indicates a continuous chemical enrichment with a short timescale less than 1 Gyr. They further suggested a possible systematic age difference among GC systems, in that the GC systems in more luminous galaxies are older. Their result related to the MDF shape is not consistent with our result that the old GCs show a bimodal metallicity distribution. In addition, their result about the systematic age difference among GC systems is not consistent with our result in the sense that the mean ages of GCs in gEs do not show any systematic dependence on the luminosity of gEs as shown in Figure 12.

Previously, several formation models of the GC systems in gEs have been suggested (Peebles 1969; Ashman & Zepf 1992; Harris et al. 1995; Forbes et al. 1997; Côté et al. 1998) and a summary of model descriptions and predictions can be found in several literature (Rhode & Zepf 2001; Lee 2003; Richtler et al. 2004; West et al. 2004; Brodie & Strader 2006; Hwang et al. 2008; Lee et al. 2010a). Considering the observational results on the kinematics and photometry of GCs in gEs and predictions of several models available in the literature, Lee et al. (2010a) presented a mixture (bibimbap) scenario describing the formation of GCs in gEs. However, they did not use the information on chemical properties and ages of GCs in gEs when they proposed their scenario. To be short, the scenario is as follows. (1) MP GCs are formed mostly in low-mass dwarf galaxies very early, and preferentially in dwarf galaxies located in the high density environment like galaxy clusters. These are the first generation

of GCs in the universe. MP GCs should be also formed in massive galaxies as well, but the number of these massive galaxies is much smaller than that of the dwarf galaxies. (2) MR GCs are formed together with stars in massive galaxies or dissipational merging galaxies later than MP GCs, but not much later than MP GCs. The chemical enrichment of the galaxies is rapid after the formation of MP GCs and the difference in the formation epoch of MP GCs and MR GCs should be small. (3) Massive galaxies grow becoming gEs via dissipationless or dissipational merging of galaxies of various types and via accretion of many dwarf galaxies. New MR GCs will be formed during the dissipational merging, but the fraction of dissipational merging at this stage should be minor. A significant fraction of MP GCs in gEs we see today are from dissipationless merging or accretion.

If we consider our results on ages and chemical properties in the view of this mixture scenario, we can conclude the followings. First, the point in the mixture scenario of Lee et al. (2010a) that MP GCs in massive galaxies are formed early is consistent with our finding that most MP GCs in gEs are older than 10 Gyr. Second, the small difference in the primary formation epochs of MP GCs and MR GCs in Lee et al. (2010a) is consistent with our results that there is little difference in the mean ages of the MP and MR sub-populations of old GCs (> 10 Gyr). Note that there is ~ 1 Gyr difference in the case of the MW GCs that have more reliable age estimates (12.9 ± 0.3 Gyr and 11.8 ± 0.2 Gyr for the MP and MR GCs, respectively).

Important findings in this study are that gEs have a significant number of young GCs and that they are mostly MR GCs. We also found that there are a smaller number of MP GCs with young ages (< 10 Gyr). The MR young GCs are probably formed during the dissipational merging of late-type galaxies with their host elliptical galaxies, while the MP young GCs are formed in dwarf galaxies and are accreted to their host galaxies. It is expected that the fraction of new MR GCs from the dissipational merging events depends on the environment such as the gas content of the merging companions and the local density where the merging happens (Park & Choi 2009; Hwang et al. 2010). Therefore, the fraction of young GCs would not be the same for all galaxies. In the case of NGC 4636, a considerable fraction of young GCs with ages less than 5 Gyr might be the result of recent merging with gaseous late-type galaxies. It would be worth investigating the environmental dependence of the GC systems in gEs once the number of gEs with spectroscopically measured metallicity and age for their GCs increases in the future.

6. Summary

We presented the measurements of the metallicity, age, and $[\alpha/\text{Fe}]$ of GCs in NGC 4636 derived from the Subaru spectroscopic data. For comparison we have also re-derived the metallicity, age, and $[\alpha/\text{Fe}]$ of GCs for six other gEs (M87, M49, M60, NGC 5128, NGC 1399, and NGC 1407) from the line indices in the literature using the same methods as used for NGC 4636 GCs. We made a combined sample of GCs in gEs by combining all the GC data in gEs including NGC 4636, and used it to investigate various properties of GCs in gEs. Final results for the combined sample as well as individual galaxies are summarized in Tables 7 – 11. Our primary results are summarized below.

1. We measured the metallicities of 59 GCs in NGC 4636 with the BH method, and the metallicity, age, and $[\alpha/\text{Fe}]$ values of 33 GCs with the grid method and χ^2 minimization method.
2. The metallicities of the NGC 4636 GCs show marginally a bimodal distribution with two peaks at $[\text{Fe}/\text{H}] = -1.23(\sigma = 0.32)$ and $-0.35(\sigma = 0.19)$ from the BH method, $-1.14(\sigma = 0.22)$ and $-0.41(\sigma = 0.21)$ from the grid method, and $-1.22(\sigma = 0.25)$ and $-0.44(\sigma = 0.16)$ from the χ^2 minimization method. The mean values of metallicity are $[\text{Fe}/\text{H}] = -0.90 \pm 0.12$ from the BH method, -0.70 ± 0.13 from the grid method, and -0.74 ± 0.11 from the χ^2 minimization method.
3. The ages of the GCs in NGC 4636 show a large range with a non-negligible number of young GCs. The mean age of the GCs is derived to be 7.9 ± 0.8 Gyr from the grid method and 8.7 ± 2.0 Gyr from the χ^2 minimization method. The number ratio for young (< 5 Gyr), intermediate ($5 - 10$ Gyr), and old (> 10 Gyr) GCs is 27:39:34 from the grid method and 27:30:43 from the χ^2 minimization method.
4. The $[\alpha/\text{Fe}]$ distribution of the NGC 4636 GCs is broad with the mean of $[\alpha/\text{Fe}] = 0.20 \pm 0.11$ from the grid method and of $[\alpha/\text{Fe}] = 0.07 \pm 0.05$ from the χ^2 minimization method, smaller than the value for the MW GCs.
5. The metallicity, age, and alpha-element of the GCs in NGC 4636 do not show any significant radial variation. NGC 4636 GCs show a hint of the age-metallicity relation.
6. The GCs in the combined sample of gEs show a bimodal metallicity distribution: peaks at $[\text{Fe}/\text{H}] = -1.21(\sigma = 0.32)$, and $-0.42(\sigma = 0.27)$ from the grid method, and $[\text{Fe}/\text{H}] = -1.25(\sigma = 0.32)$, and $-0.42(\sigma = 0.25)$ from the χ^2 minimization method. The MP GCs are on average ~ 3 Gyr older than the MR GCs. They show a large range in age from 2 to 15 Gyr, including a significant number of young GCs, while all

MW GCs are older than 7 Gyr. The MR GCs show a broader age distribution than the MP GCs, showing that young GCs are mostly metal-rich. The mean $[\alpha/\text{Fe}]$ value of the combined gE GCs is smaller than that of the MW GCs.

7. The number ratio of the young group and the old group is 1:3 for the MP GCs, and 1:1 for the MR GCs. In the case of the old group, the mean ages for the MR and MP GCs are about 13 Gyrs, and there is little difference in the mean ages between the MR and MP GCs. It is noted that the mean age for the MR GCs in the MW is about one Gyr younger than that for the MP GCs. In the case of the young group, the mean age for the MR GCs is about 5 Gyr, which is about 2 Gyr younger than that for the MP GCs.
8. The results on metallicity, age, and $[\alpha/\text{Fe}]$ of GCs in gEs as well as those on photometry and kinematics of GCs are consistent with the mixture scenario in Lee et al. (2010a).

The authors like to thank the referee for his/her useful comments which improved significantly the original manuscript. The authors are grateful to the staff of the SUBARU Telescope for their kind help during the observation. This is supported in part by the Mid-career Researcher Program through an NRF grant funded by the MEST (No.2010-0013875). H.S.H. acknowledges the support of the Smithsonian Institution.

REFERENCES

- Ashman, K. M., & Zepf, S. E. 1992, *ApJ*, 384, 50
- Ashman, K. M., Bird, C. M., & Zepf, S. E. 1994, *AJ*, 108, 2348
- Beers, T. C., Flynn, K., & Gebhardt, K. 1990, *AJ*, 100, 32
- Beasley, M. A., Sharples, R. M., Bridges, T. J., Hanes, D. A., Zepf, S. E., Ashman, K. M., & Geisler, D. 2000, *MNRAS*, 318, 1249
- Beasley, M. A., Bridges, T., Peng, E. W., Harris, W. E., Harris, G. L. H., Forbes, D. A., & Mackie, G. 2008, *MNRAS*, 386, 1443
- Bellini, A., Bedin, L. R., Piotto, G., et al. 2010, *AJ*, 140, 631
- Brodie, J. P., & Huchra J. P. 1990, *ApJ*, 362, 503 (BH)
- Brodie, J. P., Strader, J., Denicoló, G., et al. 2005, *AJ*, 129, 2643

- Brodie, J. P., & Strader, J. 2006, *ARA&A*, 44, 193
- Burstein, D., Faber, S. M., Gaskell, C. M., & Krumm, N. 1984, *ApJ*, 287, 586
- Carretta, E., Bragaglia, A., Gratton, R. G., Recio-Blanco, A., Lucatello, S., D’Orazi, V., & Cassisi, S. 2010, *A&A*, 516, A55
- Cenarro, A. J., Beasley, M. A., Strader, J., Brodie, J. P., & Forbes, D. A. 2007, *AJ*, 134, 391
- Chakrabarty, D., & Raychaudhury, S. 2008, *AJ*, 135, 2350
- Chies-Santos, A. L., Larsen, S. S., Cantiello, M., et al. 2012, *A&A*, 539, A54
- Cohen, J. G., Blakeslee, J. P., & Ryzhov, A. 1998, *ApJ*, 496, 808
- Cohen, J. G., Blakeslee, J. P., & Côté, P. 2003, *ApJ*, 592, 866
- Colucci, J. E., Bernstein, R. A., Cameron, S. A., & McWilliam, A. 2011, *ApJ*, 735, 55
- Côté, P., Marzke, R.O., & West, M.J. 1998, *ApJ*, 501, 554
- Dirsch, B., Schuberth, Y., & Richtler, T. 2005, *A&A*, 433, 43
- Dotter, A., Sarajedini, A., Anderson, J., et al. 2010, *ApJ*, 708, 698
- Forbes D.A., Brodie J.P., & Grillmair C.J. 1997, *AJ*, 113, 1652
- Forbes, D. A., Beasley, M. A., Brodie, J. P., & Kissler-Patig, M. 2001, *ApJ*, 563, L143
- Harris, W. E., Pritchett, C. J., & McClure, R. D. 1995, *ApJ*, 441, 120
- Harris, W. E. 1996, *AJ*, 112, 1487 (2010 version)
- Huchra, J. P., et al. 1996, *ApJS*, 102, 29
- Hwang, H. S., et al. 2008, *ApJ*, 674, 869
- Hwang, H. S., Elbaz, D., Lee, J. C., et al. 2010, *A&A*, 522, A33
- Kashikawa, N., et al. 2002, *PASP*, 54, 819
- Kim, E., Kim, D.-W., Fabbiano, G., Lee, M. G., Park, H. S., Geisler, D., & Dirsch, B. 2006, *ApJ*, 647, 276
- Kim, S. C., Lee, M. G., Geisler, D., Sarajedini, A., Park, H. S., Hwang, H. S., Harris, W. E., Seguel, J. C., & von Hippel, T. 2007, *AJ*, 134, 706

- Kissler-Patig, M., Brodie, J. P., Schroder, L. L., Forbes, D. A., Grillmair, C. J., & Huchra, J. P. 1998, *AJ*, 115, 105
- Kissler, M., Richtler, T., Held, E. V., Grebel, E. K., Wagner, S. J., & Capaccioli, M. 1994, *A&A*, 287, 463
- Kuntschner, H., Lucey, J. R., Smith, R. J., Hudson, M. J., & Davies, R. L. 2001, *MNRAS*, 323, 615
- Kuntschner, H., Ziegler, B. L., Sharples, R. M., Worthey, G., & Fricke, K. J. 2002, *A&A*, 395, 761
- Lee, J.-W., Kang, Y.-W., Lee, J., & Lee, Y.-W. 2009, *Nature*, 462, 480
- Lee, M. G. 2003, *Jour. Korean Astron. Soc.*, 36, 189
- Lee, M. G., Park, H. S., Kim, E., Hwang, H. S., Kim, S. C., & Geisler, D. 2008a, *ApJ*, 682, 135
- Lee, M. G., et al. 2008b, *ApJ*, 674, 857
- Lee, M. G., Hwang, H. S., Kim, S. C., Park, H. S., Geisler, D., Sarajedini, A., & Harris, W. E. 2008c, *ApJ*, 674, 886
- Lee, M. G., Park, H. S., Hwang, H. S., Arimoto, N., Tamura, N., & Onodera, M. 2010a, *ApJ*, 709, 1083
- Lee, M. G., Park, H. S., & Hwang, H. S. 2010b, *Science*, 328, 334
- Marín-Franch, A., et al. 2009, *ApJ*, 694, 1498
- Marino, A. F., Milone, A. P., Piotto, G., et al. 2009, *A&A*, 505, 1099
- Muratov, A. L., & Gnedin, O. Y. 2010, *ApJ*, 718, 1266
- Park, C., & Choi, Y.-Y. 2009, *ApJ*, 691, 1828
- Park, H. S., Lee, M. G., Hwang, H. S., Arimoto, N., Tamura, N., & Onodera, M. 2010, *ApJ*, 709, 377
- Park, H. S., et al. 2012a, in preparation
- Park, H. S., Lee, M. G. & Hwang, H. S. 2012b, *ApJ*, in press

- Paturel G., Petit C., Prugniel P., Theureau G., Rousseau J., Brouty M., Dubois P., Cambrésy L., 2003, *A&A*, 412, 45
- Paudel, S., Lisker, T., Kuntschner, H., Grebel, E. K., & Glatt, K. 2010, *MNRAS*, 405, 800
- Peebles, P. J. E. 1969, *ApJ*, 155, 393
- Peng, E. W., Ford, H. C., & Freeman, K. C. 2004, *ApJ*, 602, 705
- Peng, E. W., Jordán, A., Côté, P., et al. 2006, *ApJ*, 639, 95
- Pierce, M., et al. 2006, *MNRAS*, 368, 325
- Posson-Brown, J., Raychaudhury, S., Forman, W., Donnelly, R. H., & Jones, C. 2009, *ApJ*, 695, 1094
- Proctor, R. N., Forbes, D. A., & Beasley, M. A. 2004, *MNRAS*, 355, 1327
- Puzia, T. H., Zepf, S. E., Kissler-Patig, M., Hilker, M., Minniti, D., & Goudfrooij, P. 2002, *A&A*, 391, 453
- Puzia, T. H., Perrett, K. M., & Bridges, T. J. 2005a, *A&A*, 434, 909
- Puzia, T. H., Kissler-Patig, M., Thomas, D., et al. 2005b, *A&A*, 439, 997
- Rhode, K. L., & Zepf, S. E. 2001, *AJ*, 121, 210
- Richtler, T., et al. 2004, *AJ*, 127, 2094
- Schuberth, Y., Richtler, T., Dirsch, B., Hilker, M., Larsen, S. S., Kissler-Patig, M., & Mebold, U. 2006, *A&A*, 459, 391
- Sharina, M. E., Chandar, R., Puzia, T. H., Goudfrooij, P., & Davoust, E. 2010, *MNRAS*, 405, 839
- Spitler, L. R., Forbes, D. A., & Beasley, M. A. 2008, *MNRAS*, 389, 1150
- Thomas, D., Greggio, L., & Bender, R. 1999, *MNRAS*, 302, 537
- Thomas, D., Maraston, C., & Bender, R. 2003, *MNRAS*, 339, 897
- Thomas, D., Maraston, C., & Korn, A. 2004, *MNRAS*, 351, L19
- Thomas, D., Maraston, C., Bender, R., & Mendes de Oliveira, C. 2005, *ApJ*, 621, 673
- Trager, S. C., Worthey, G., Faber, S. M., Burstein, D., & Gonzalez, J. J. 1998, *ApJS*, 116, 1

- Trager, S. C., Faber, S. M., Worthey, G., & González, J. J., 2000, *AJ*, 119, 1645
- Trager, S. C. 2004, *Origin and Evolution of the Elements*, 388
- Trager, S. C., Faber, S. M., & Dressler, A. 2008, *MNRAS*, 386, 715
- Tripicco M., & Bell R. A., 1995, *AJ*, 110, 3035
- West, M. J., Côté, P., Marzke, R. O., & Jordan, A. 2004, *Nature*, 427, 31
- Woodley, K. A., Harris, W. E., Puzia, T. H., Gómez, M., Harris, G. L. H, & Geisler, D. 2010
ApJ, 708, 1335
- Woodley, K. A., & Gómez, M. 2010, *PASA*, 27, 379
- Worthey, G. 1994, *ApJS*, 95, 107
- Worthey, G., & Ottaviani, D. L. 1997, *ApJS*, 111, 377
- Yoon, S.-J., Yi, S. K., & Lee, Y.-W. 2006, *Science*, 111, 1129
- Yoon, S.-J., Sohn, S. T., Lee, S.-Y., et al. 2011a, *ApJ*, 743, 149
- Yoon, S.-J., Lee, S.-Y., Blakeslee, J. P., et al. 2011b, *ApJ*, 743, 150

Table 1. Zero Point Offsets for Lick Index calibration

index	unit	offset ^a	rms
CN1	mag	−0.021	0.004
CN2	mag	−0.007	0.018
Ca4227	Å	0.021	0.367
G4300	Å	0.414	0.249
Fe4383	Å	0.515	0.259
Ca4455	Å	0.408	0.291
Fe4531	Å	0.842	0.780
C24668	Å	−1.880	1.036
H β	Å	0.184	0.140
Fe5015	Å	0.616	0.267
Mg1	mag	−0.017	0.016
Mg2	mag	−0.015	0.018
Mgb	Å	0.165	0.187
Fe5270	Å	0.443	0.306
Fe5335	Å	−0.103	0.162
Fe5406	Å	0.271	0.147
Fe5709	Å	0.148	0.484
Fe5782	Å	0.036	0.156
NaD	Å	0.494	0.578
H δ_A	Å	−0.367	0.458
H γ_A	Å	−0.761	0.645
H δ_F	Å	0.129	0.242
H γ_F	Å	0.083	0.269

^a $Index(\text{Lick}) = Index(\text{Subaru}) + constant.$

Table 2. Lick Line Indices (set 1)

ID ^a	CN1 (mag)	CN2 (mag)	Ca4227 (Å)	G4300 (Å)	Fe4383 (Å)	Ca4455 (Å)	Fe4531 (Å)	C24668 (Å)	H β (Å)	Fe5015 (Å)	Mg1 (mag)	Mg2 (mag)
157	0.219	0.242	0.747	4.612	6.693	-0.054	4.808	-2.320	1.865	4.851	0.093	0.219
182	-0.070	-0.030	1.912	0.824	-1.213	0.581	0.719	-3.783	1.935	-0.530	0.001	0.073
244	0.290	0.322	-3.348	6.267	5.615	3.151	1.416	-0.785	2.230	3.279	0.056	0.233
...												

^a From Park et al. (2010, 2012a)

Note. — This table is available in its entirety in amachine-readable form in the online journal. A portion is shown here for guidance regarding its form and content.

Table 3. Lick Line Indices (set 2)

ID ^a	Mgb (Å)	Fe5270 (Å)	Fe5335 (Å)	Fe5406 (Å)	Fe5709 (Å)	Fe5782 (Å)	NaD (Å)	H δ_A (Å)	H γ_A (Å)	H δ_F (Å)	H γ_F (Å)
157	3.837	2.943	2.952	2.993	1.325	0.556	1.426	-3.797	-5.303	-0.301	-0.951
182	0.322	1.199	2.723	-0.436	0.916	0.360	5.777	-0.220	3.506	-0.837	2.851
244	5.220	0.723	2.289	1.335	1.666	-0.001	1.963	-3.485	-17.252	-1.465	-7.051
...											

^a From Park et al. (2010, 2012a)

Note. — This table is available in its entirety in amachine-readable form in the online journal. A portion is shown here for guidance regarding its form and content.

Table 4. Lick Index Errors (set 1)

ID ^a	CN1 (mag)	CN2 (mag)	Ca4227 (Å)	G4300 (Å)	Fe4383 (Å)	Ca4455 (Å)	Fe4531 (Å)	C24668 (Å)	H β (Å)	Fe5015 (Å)	Mg1 (mag)	Mg2 (mag)
157	0.024	0.031	0.502	0.931	1.217	0.553	0.898	1.341	0.447	1.013	0.014	0.016
182	0.019	0.025	0.404	0.790	1.188	0.502	0.916	1.367	0.439	1.019	0.014	0.016
244	0.028	0.036	0.614	1.168	1.513	0.633	1.082	1.574	0.502	1.143	0.016	0.012
...												

^a From Park et al. (2010, 2012a)

Note. — This table is available in its entirety in amachine-readable form in the online journal. A portion is shown here for guidance regarding its form and content.

Table 5. Lick Index Errors (set 2)

ID ^a	Mgb (Å)	Fe5270 (Å)	Fe5335 (Å)	Fe5406 (Å)	Fe5709 (Å)	Fe5782 (Å)	NaD (Å)	H δ_A (Å)	H γ_A (Å)	H δ_F (Å)	H γ_F (Å)
157	0.457	0.461	0.581	0.394	0.275	0.266	0.424	1.013	0.756	0.647	0.438
182	0.435	0.454	0.567	0.409	0.275	0.278	0.423	0.848	0.655	0.562	0.397
244	0.516	0.525	0.678	0.444	0.308	0.289	0.437	1.148	0.918	0.751	0.508
...											

^a From Park et al. (2010, 2012a)

Note. — This table is available in its entirety in amachine-readable form in the online journal. A portion is shown here for guidance regarding its form and content.

Table 6. Metallicity, Age, and $[\alpha/\text{Fe}]$ of NGC 4636 GCs

ID ^a	$[\text{Z}/\text{H}]_{grid}^{[MgFe]’}$ (dex)	$[\text{Z}/\text{H}]_{grid}^{Mg2}$ (dex)	Age _{grid} (Gyr)	$[\alpha/\text{Fe}]_{grid}$ (dex)	$[\text{Z}/\text{H}]_{\chi^2}$ (dex)	Age _{χ^2} (Gyr)	$[\alpha/\text{Fe}]_{\chi^2}$ (dex)	$[\text{Fe}/\text{H}]_{BH}$ (dex)
157	0.27 ± 0.28	0.11 ± 0.05	4.7 ± 3.9	-0.08 ± 0.10	0.11 ± 0.09	7.0 ± 2.6	-0.20 ± 0.12	-0.13 ± 0.16
182	-1.70 ± 0.39	-1.04 ± 0.10	14.0 ± 1.5	-0.30 ± 0.00	-1.46 ± 0.23	12.0 ± 3.6	-0.30 ± 0.25	-1.79 ± 0.16
244	-0.21 ± 0.22	-0.12 ± 0.05	5.4 ± 4.0	0.49 ± 0.02	0.23 ± 0.09	2.2 ± 0.8	0.26 ± 0.21	-0.32 ± 0.48
...								

^a From Park et al. (2010, 2012a)

Note. — This table is available in its entirety in amachine-readable form in the online journal. A portion is shown here for guidance regarding its form and content.

Table 7. KMM Test Results for the Metallicities of GCs in gEs^a

galaxy	N	$[\text{Fe}/\text{H}]_{MP} \pm \sigma$ (dex)	N	$[\text{Fe}/\text{H}]_{MR} \pm \sigma$ (dex)	confidence level (%)
<u>grid method</u>					
NGC 4636	10	-1.14 ± 0.22	15	-0.41 ± 0.21	71.4
NGC 5128	42	-1.14 ± 0.32	14	-0.34 ± 0.12	97.7
M60	5	-1.27 ± 0.62	33	-0.56 ± 0.36	71.9
NGC 1407	7	-1.14 ± 0.23	12	-0.38 ± 0.18	76.2
NGC 1399	3	-1.63 ± 0.06	7	-0.25 ± 0.51	94.6
M87	66	-1.24 ± 0.32	63	-0.45 ± 0.27	97.5
M49	28	-0.82 ± 0.65	15	0.37 ± 0.10	99.9
gEs	155	-1.21 ± 0.32	149	-0.42 ± 0.27	99.9
gEs (≤ 10 Gyr)	22	-1.41 ± 0.14	94	-0.57 ± 0.37	98.4
gEs (> 10 Gyr)	111	-1.22 ± 0.34	77	-0.42 ± 0.25	99.7
<u>χ^2 minimization method</u>					
NGC 4636	14	-1.22 ± 0.25	14	-0.44 ± 0.16	95.2
NGC 5128	43	-1.40 ± 0.47	19	-0.43 ± 0.15	98.2
M60	20	-1.09 ± 0.31	15	-0.37 ± 0.11	98.8
NGC 1407	8	-1.05 ± 0.33	11	-0.39 ± 0.11	92.8
NGC 1399	4	-1.68 ± 0.24	6	-0.37 ± 0.21	94.5
M87	40	-1.41 ± 0.14	90	-0.67 ± 0.36	99.9
M49	26	-1.15 ± 0.71	20	0.19 ± 0.25	99.2
gEs	167	-1.25 ± 0.32	148	-0.42 ± 0.25	99.9
gEs (≤ 10 Gyr)	63	-1.11 ± 0.43	64	-0.32 ± 0.27	98.5
gEs (> 10 Gyr)	114	-1.25 ± 0.29	74	-0.44 ± 0.18	99.9
MW ^b	111	-1.52 ± 0.39	41	-0.52 ± 0.23	99.8

^a Peak values, widths (σ), and confidence levels are derived from the KMM test.

^b It is from Harris (1996).

Table 8. Mean Metallicities of GCs in gEs^a

galaxy	N	total <[Fe/H]> ± <σ> (dex)	N	age ≤ 10 Gyr <[Fe/H]> ± <σ> (dex)	N	age > 10 Gyr <[Fe/H]> ± <σ> (dex)	N	[α/Fe] ≤ 0.2 <[Fe/H]> ± <σ> (dex)	N	[α/Fe] > 0.2 <[Fe/H]> ± <σ> (dex)
<u>grid method</u>										
NGC 4636	33	-0.70 ± 0.13	22	-0.49 ± 0.14	11	-1.20 ± 0.25	17	-0.50 ± 0.18	16	-0.86 ± 0.21
NGC 5128	68	-1.10 ± 0.08	23	-0.81 ± 0.11	45	-1.27 ± 0.11	44	-1.07 ± 0.11	24	-1.14 ± 0.13
M60	38	-0.67 ± 0.08	10	-0.93 ± 0.20	28	-0.59 ± 0.09	24	-0.70 ± 0.09	14	-0.58 ± 0.18
NGC 1407	20	-0.68 ± 0.13	4	-0.48 ± 0.20	16	-0.74 ± 0.15	1	-2.39 ± 0.16	19	-0.65 ± 0.13
NGC 1399	10	-0.66 ± 0.27	7	-0.33 ± 0.47	3	-1.60 ± 0.43	7	-0.93 ± 0.49	3	0.32 ± 0.62
M87	146	-0.83 ± 0.06	56	-0.57 ± 0.08	90	-1.00 ± 0.07
M49	43	-0.42 ± 0.14	20	-0.10 ± 0.34	23	-0.68 ± 0.20	30	-0.48 ± 0.16	13	-0.22 ± 0.30
gEs	358	-0.80 ± 0.04	142	-0.55 ± 0.05	216	-0.96 ± 0.05	123	-0.78 ± 0.08	89	-0.76 ± 0.08
<u>χ² minimization method</u>										
NGC 4636	33	-0.74 ± 0.11	19	-0.59 ± 0.16	14	-0.94 ± 0.14	20	-0.92 ± 0.13	13	-0.40 ± 0.11
NGC 5128	62	-1.15 ± 0.08	21	-1.11 ± 0.14	41	-1.17 ± 0.09	46	-1.20 ± 0.10	16	-1.01 ± 0.14
M60	38	-0.76 ± 0.09	11	-0.58 ± 0.26	27	-0.82 ± 0.11	16	-0.75 ± 0.15	22	-0.76 ± 0.13
NGC 1407	20	-0.62 ± 0.13	6	-0.52 ± 0.16	14	-0.69 ± 0.17	6	-0.91 ± 0.19	14	-0.44 ± 0.12
NGC 1399	10	-0.83 ± 0.40	7	-0.51 ± 0.36	3	-1.16 ± 0.79	5	-1.48 ± 0.78	5	-0.56 ± 0.20
M87	150	-0.90 ± 0.05	52	-0.63 ± 0.08	98	-1.08 ± 0.06	77	-1.02 ± 0.07	73	-0.77 ± 0.08
M49	46	-0.58 ± 0.16	24	-0.44 ± 0.18	22	-0.77 ± 0.25	23	-0.69 ± 0.19	23	-0.38 ± 0.29
gEs	359	-0.86 ± 0.04	140	-0.65 ± 0.06	219	-1.00 ± 0.04	193	-1.00 ± 0.05	166	-0.70 ± 0.05
MW	152	-1.28 ± 0.05	3	-0.61 ± 0.27	61	-1.44 ± 0.08	8	-1.33 ± 0.30	49	-1.40 ± 0.10

^a The mean values are determined with the biweight location of Beers et al. (1990). The uncertainties, <σ>, indicate the 68% confidence levels obtained with a bootstrap method.

Table 9. Mean Ages of GCs in gEs^a

galaxy	N	total		[Fe/H] ≤ -0.9		[Fe/H] > -0.9		[α/Fe] ≤ 0.2		[α/Fe] > 0.2	
		<age> ± <σ> (Gyr)	N	<age> ± <σ> (Gyr)							
<u>grid method</u>											
NGC 4636	33	7.9 ± 0.8	13	12.3 ± 2.1	20	6.4 ± 1.0	17	7.5 ± 1.3	16	8.2 ± 1.0	
NGC 5128	68	12.3 ± 0.5	42	12.4 ± 0.4	26	10.1 ± 1.8	44	12.3 ± 0.6	24	12.3 ± 0.5	
M60	38	13.0 ± 0.0	12	12.9 ± 1.6	26	13.0 ± 0.3	24	13.0 ± 0.3	14	12.6 ± 0.6	
NGC 1407	20	12.6 ± 0.3	8	12.0 ± 0.2	12	13.0 ± 0.1	1	13.0 ± 0.3	19	12.5 ± 0.4	
NGC 1399	10	6.9 ± 1.5	3	12.5 ± 4.0	7	5.5 ± 1.6	7	7.6 ± 1.7	3	4.9 ± 4.8	
M87	146	12.4 ± 0.2	66	12.1 ± 0.2	80	8.8 ± 2.2	
M49	43	9.5 ± 2.1	13	12.1 ± 0.2	30	7.7 ± 1.2	30	8.0 ± 1.3	13	12.2 ± 0.6	
gEs	358	12.3 ± 0.1	157	12.2 ± 0.1	201	9.2 ± 0.7	123	12.4 ± 1.5	89	12.2 ± 0.2	
<u>χ² minimization method</u>											
NGC 4636	33	8.7 ± 2.0	14	11.9 ± 1.5	19	7.3 ± 1.2	20	9.0 ± 1.0	13	8.2 ± 3.4	
NGC 5128	62	12.1 ± 0.4	40	12.3 ± 0.3	22	11.9 ± 1.3	46	12.4 ± 0.5	16	11.5 ± 1.0	
M60	38	12.9 ± 0.3	16	12.6 ± 0.4	22	13.0 ± 0.6	16	12.7 ± 1.3	22	12.8 ± 0.2	
NGC 1407	20	12.8 ± 0.5	6	12.9 ± 0.3	14	12.6 ± 1.4	6	10.0 ± 2.1	14	13.0 ± 0.2	
NGC 1399	10	7.5 ± 1.8	4	11.5 ± 2.0	6	5.1 ± 1.7	5	9.5 ± 3.3	5	4.8 ± 2.6	
M87	150	12.3 ± 0.1	75	12.2 ± 0.1	75	11.7 ± 2.1	77	12.3 ± 0.1	73	12.4 ± 0.1	
M49	46	9.5 ± 1.5	18	11.7 ± 1.0	28	8.6 ± 1.2	23	9.0 ± 1.0	23	11.8 ± 1.5	
gEs	359	12.2 ± 0.1	173	12.2 ± 0.1	186	9.7 ± 0.7	193	12.2 ± 0.1	166	12.3 ± 0.1	
MW	64	12.2 ± 0.1	48	12.9 ± 0.3	16	11.8 ± 0.2	6	10.7 ± 1.0	38	13.0 ± 0.2	

^a The mean values are determined with the biweight location of Beers et al. (1990). The uncertainties, <σ>, indicate the 68% confidence levels obtained with a bootstrap method.

Table 10. Mean $[\alpha/\text{Fe}]$ s of GCs in gEs^a

galaxy	N	total $\langle[\alpha/\text{Fe}] \pm \sigma \rangle$ (dex)	N	$[\text{Fe}/\text{H}] \leq -0.9$ $\langle[\alpha/\text{Fe}] \pm \sigma \rangle$ (dex)	N	$[\text{Fe}/\text{H}] > -0.9$ $\langle[\alpha/\text{Fe}] \pm \sigma \rangle$ (dex)	N	age ≤ 10 Gyr $\langle[\alpha/\text{Fe}] \pm \sigma \rangle$ (dex)	N	age > 10 Gyr $\langle[\alpha/\text{Fe}] \pm \sigma \rangle$ (dex)
<u>grid method</u>										
NGC 4636	33	0.20 ± 0.11	13	0.48 ± 0.15	20	0.17 ± 0.06	22	0.22 ± 0.14	11	0.17 ± 0.20
NGC 5128	68	0.13 ± 0.03	42	0.14 ± 0.04	26	0.12 ± 0.05	23	0.14 ± 0.05	45	0.12 ± 0.04
M60	38	0.06 ± 0.04	12	0.01 ± 0.22	26	0.08 ± 0.05	10	-0.08 ± 0.15	28	0.09 ± 0.05
NGC 1407	20	0.42 ± 0.05	8	0.44 ± 0.05	12	0.40 ± 0.06	4	0.36 ± 0.06	16	0.46 ± 0.05
NGC 1399	10	0.07 ± 0.09	3	-0.30 ± 0.19	7	0.21 ± 0.08	7	0.09 ± 0.10	3	0.09 ± 0.39
M87
M49	43	0.09 ± 0.04	13	-0.04 ± 0.19	30	0.13 ± 0.05	20	0.02 ± 0.05	23	0.15 ± 0.07
gEs	212	0.14 ± 0.02	91	0.14 ± 0.03	121	0.15 ± 0.02	86	0.12 ± 0.03	126	0.16 ± 0.02
<u>χ^2 minimization method</u>										
NGC 4636	33	0.07 ± 0.05	14	-0.10 ± 0.07	19	0.21 ± 0.07	19	0.05 ± 0.06	14	0.10 ± 0.11
NGC 5128	62	0.06 ± 0.03	40	0.02 ± 0.04	22	0.12 ± 0.03	21	0.07 ± 0.06	41	0.05 ± 0.03
M60	38	0.26 ± 0.05	16	0.36 ± 0.15	22	0.26 ± 0.03	11	0.24 ± 0.08	27	0.28 ± 0.05
NGC 1407	20	0.31 ± 0.03	6	0.21 ± 0.13	14	0.33 ± 0.04	6	0.25 ± 0.07	14	0.33 ± 0.04
NGC 1399	10	0.15 ± 0.09	4	-0.25 ± 0.15	6	0.32 ± 0.15	7	0.18 ± 0.19	3	0.17 ± 0.18
M87	150	0.16 ± 0.02	75	0.05 ± 0.04	75	0.24 ± 0.02	52	0.21 ± 0.04	98	0.13 ± 0.03
M49	46	0.19 ± 0.04	18	0.11 ± 0.14	28	0.24 ± 0.04	24	0.17 ± 0.06	22	0.23 ± 0.11
gEs	359	0.16 ± 0.01	173	0.07 ± 0.02	186	0.23 ± 0.01	140	0.16 ± 0.02	219	0.15 ± 0.02
MW	57	0.36 ± 0.01	43	0.38 ± 0.01	14	0.29 ± 0.04	2	-0.02 ± 0.01	42	0.37 ± 0.01

^a The mean values are determined with the biweight location of Beers et al. (1990). The uncertainties, $\langle \sigma \rangle$, indicate the 68% confidence levels obtained with a bootstrap method.

Table 11. Mean Age and Metallicity of GCs in gEs and the MW^a

	young GC (age \leq 10 Gyr)			old GC (age $>$ 10 Gyr)		
	N	\langle [Fe/H] \rangle (dex)	\langle age \rangle (Gyr)	N	\langle [Fe/H] \rangle (dex)	\langle age \rangle (Gyr)
	<u>gEs (grid)</u>					
MP GC ([Fe/H] \leq -0.9)	42	-1.26 ± 0.04	7.0 ± 0.3	115	-1.41 ± 0.06	12.5 ± 0.4
MR GC ([Fe/H] $>$ -0.9)	100	-0.27 ± 0.05	4.8 ± 0.3	101	-0.45 ± 0.03	13.0 ± 0.3
	<u>gEs (χ^2 minimization)</u>					
MP GC ([Fe/H] \leq -0.9)	50	-1.33 ± 0.05	7.2 ± 0.3	123	-1.39 ± 0.06	12.5 ± 0.5
MR GC ([Fe/H] $>$ -0.9)	90	-0.32 ± 0.04	5.1 ± 0.3	96	-0.48 ± 0.03	13.0 ± 0.3
	<u>MW</u>					
MP GC ([Fe/H] \leq -0.9)	0	48	-1.64 ± 0.05	12.9 ± 0.3
MR GC ([Fe/H] $>$ -0.9)	3	-0.61 ± 0.26	7.0 ± 0.8	13	-0.60 ± 0.06	11.8 ± 0.3

^a The mean values are determined with the biweight location of Beers et al. (1990). The uncertainties indicate the 68% confidence levels obtained with a bootstrap method.

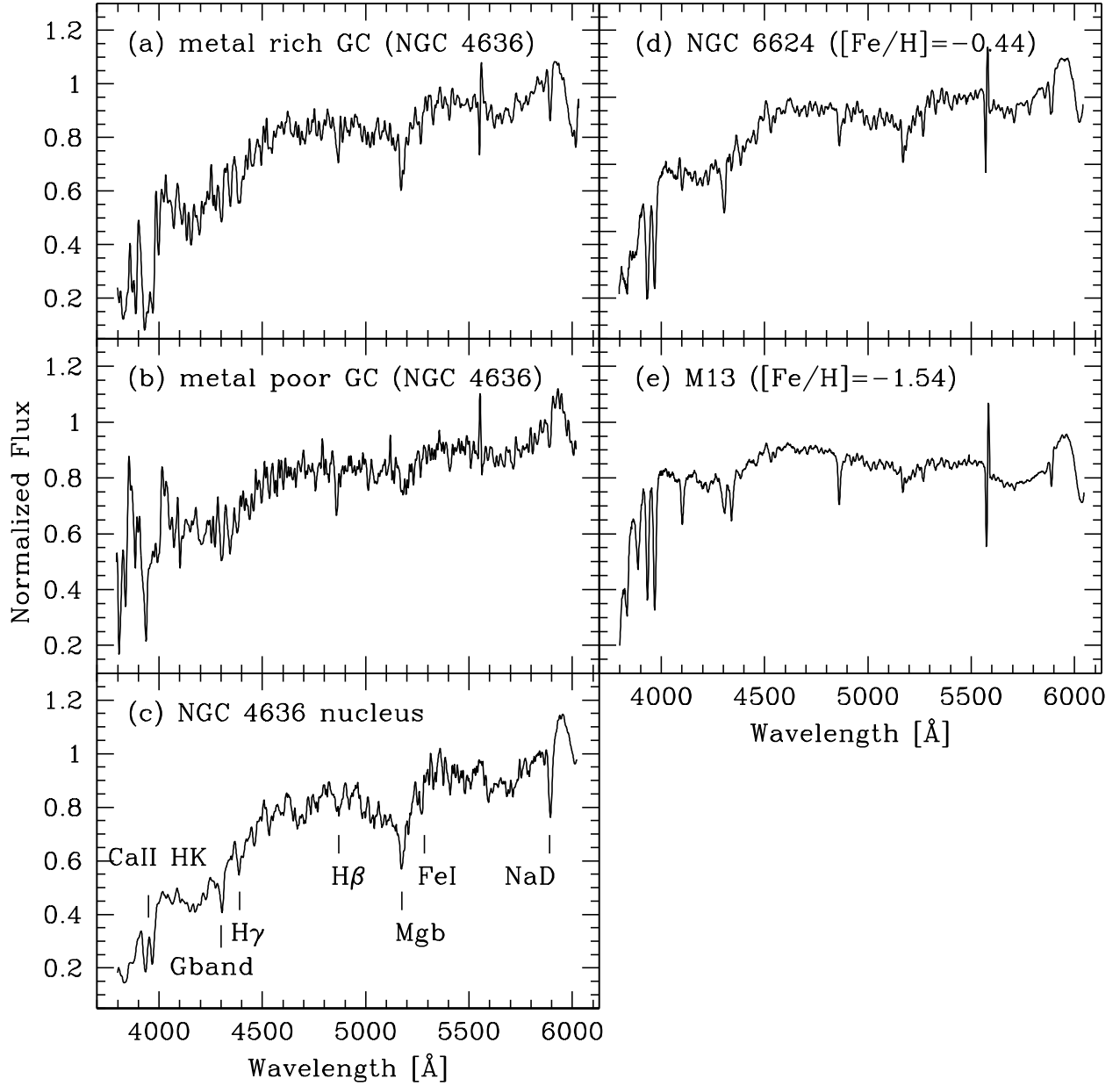


Fig. 1.— Example spectra of (a) a metal-rich (MR) GC in NGC 4636 (ID: 154) with $T_1 = 19.82$ and $[\text{Fe}/\text{H}] = -0.39$ dex; (b) a metal-poor (MP) GC in NGC 4636 (ID: 9995) with $T_1 = 19.22$ and $[\text{Fe}/\text{H}] = -1.49$ dex; (c) NGC 4636 nucleus; (d) NGC 6624, a MR MW GC with $[\text{Fe}/\text{H}] = -0.44$ dex; and (e) M13, a MP MW GC with $[\text{Fe}/\text{H}] = -1.54$ dex. All spectra are plotted in the rest frame and are smoothed with the Lick resolution.

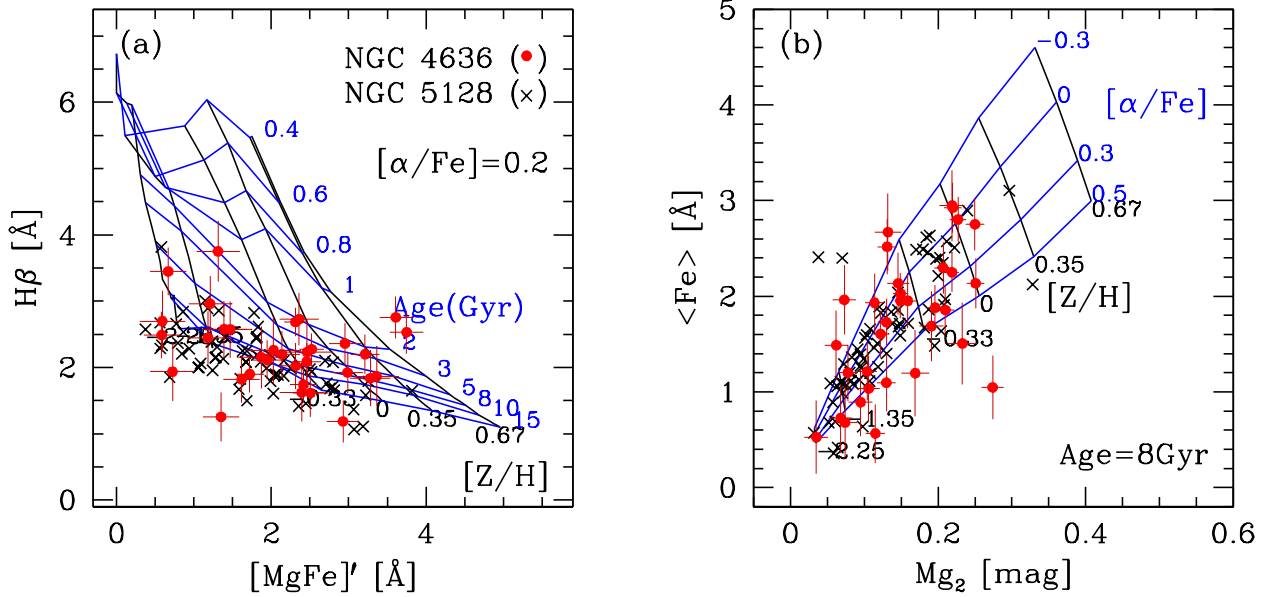


Fig. 2.— Lick line index diagrams. (a) $H\beta$ line versus $[MgFe]'$ for NGC 4636 GCs measured in this study (circles). The crosses represents NGC 5128 GCs (Woodley et al. 2010). The grids represent the SSP models for various values of $[Z/H]$ (-2.25 , -1.35 , -0.33 , 0 , 0.35 , and 0.67) and ages (0.4 , 0.6 , 0.8 , 1 , 2 , 3 , 5 , 8 , 10 , and 15 Gyr) given by Thomas et al. (2003, 2004). (b) $\langle Fe \rangle$ versus Mg_2 . The grids are for a model age of 8 Gyr.

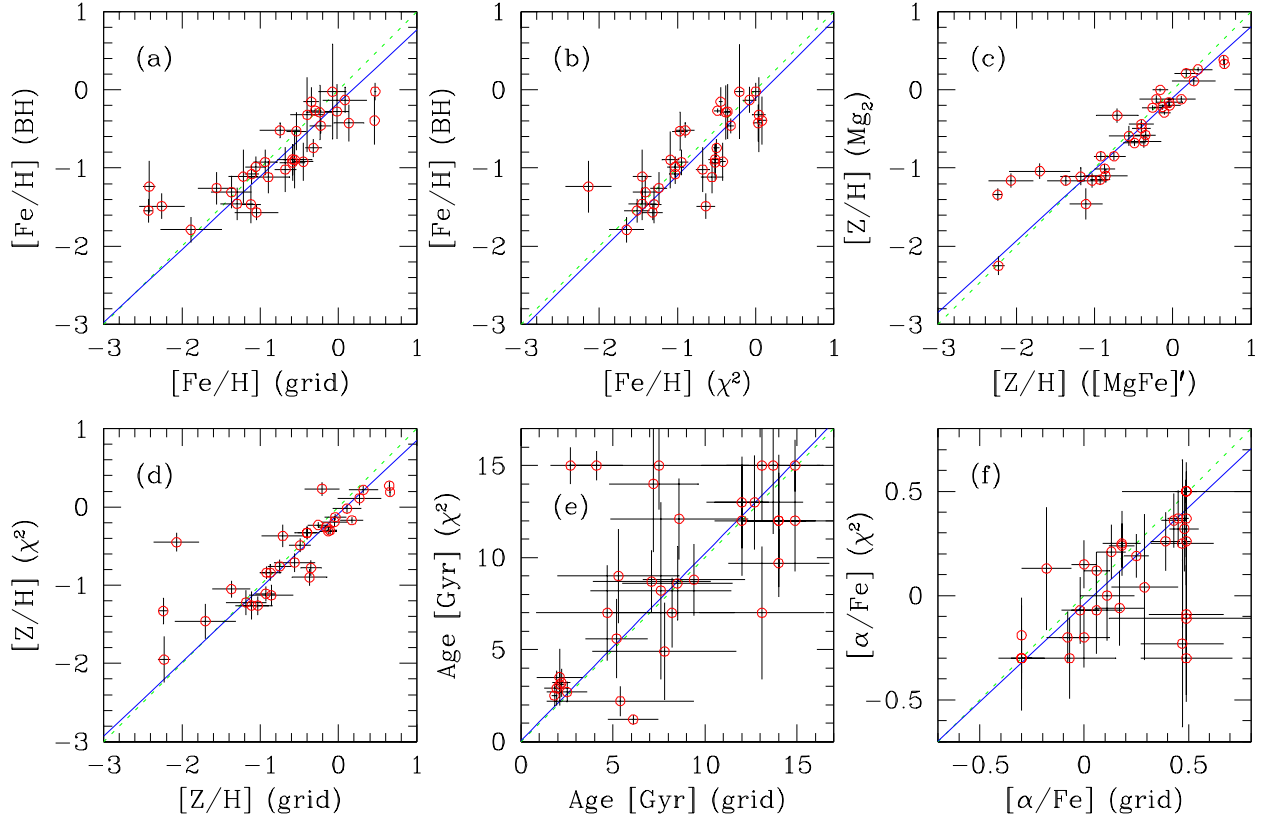


Fig. 3.— (a) Comparison of metallicities for NGC 4636 GCs measured with the BH method and with the grid method. Here the grid metallicities are the values derived from the $H\beta$ versus $[MgFe]'$ grid. (b) Comparison of $[Fe/H]$ for NGC 4636 GCs measured with the BH method and the χ^2 minimization method (c) Comparison of $[Z/H]$ values obtained from Mg_2 grids and $[MgFe]'$ grids. Comparison of parameters for NGC 4636 GCs measured with the grid method and the χ^2 minimization method: (d) $[Z/H]$, (e) age, and (f) $[\alpha/Fe]$. Here the grid metallicities are the values derived from the $H\beta$ versus $[MgFe]'$ grid. The solid and dotted lines represent the linear least-squares fit with 2σ clipping and the one-to-one relation, respectively.

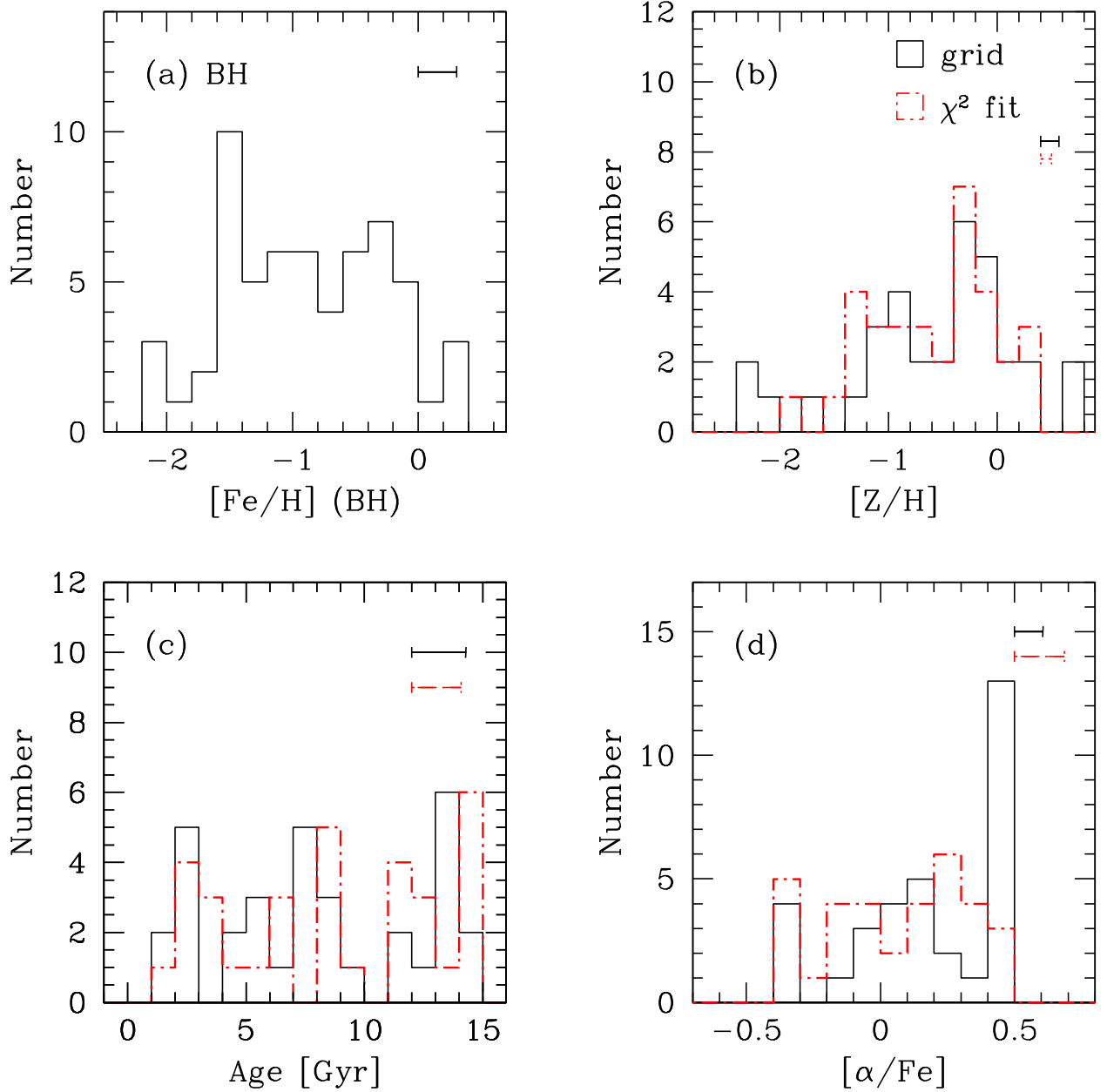


Fig. 4.— Metallicity, age, and $[\alpha/\text{Fe}]$ distribution for NGC 4636 GCs. (a) Distribution of $[\text{Fe}/\text{H}]$ from the BH method. (b) $[\text{Z}/\text{H}]$ distributions obtained from $\text{H}\beta$ versus $[\text{MgFe}]'$ grid. (c) Age distribution. (d) $[\alpha/\text{Fe}]$ distribution. The solid and dot-dashed histograms represent the distributions derived with grid and χ^2 method, respectively. The error bars in the upper right of each panel indicate the mean error of each value.

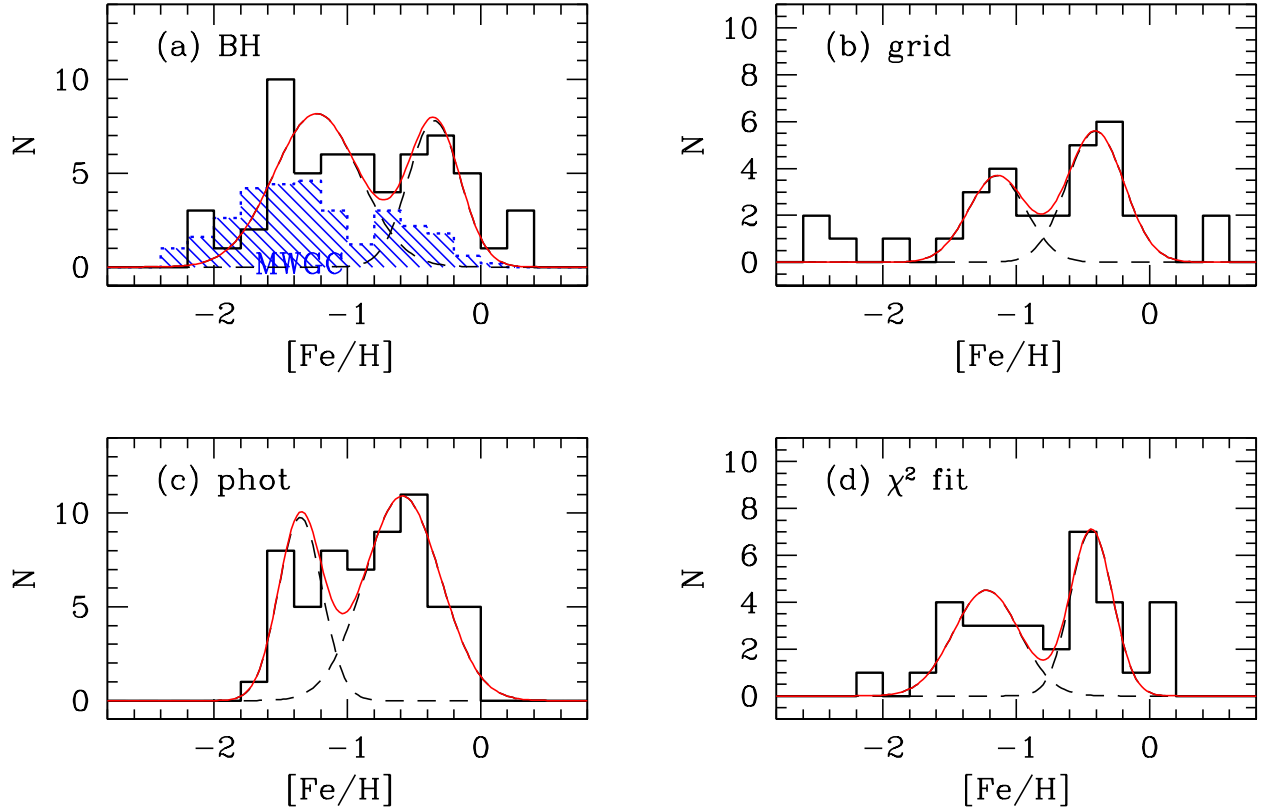


Fig. 5.— Metallicity distribution of NGC 4636 GCs. (a) $[Fe/H]$ distribution from the BH method. The hatched histogram represents the $[Fe/H]$ distribution of the MW GCs (Harris 1996). The histograms in (b) and (d) represent $[Fe/H]$ distributions obtained from the grid and χ^2 minimization method, respectively. (c) Photometric metallicity distribution obtained from $(C - T_1)_0$ by Park et al. (2012a) and the double linear equation by Lee et al. (2008a). The curved solid lines represent double Gaussian fits.

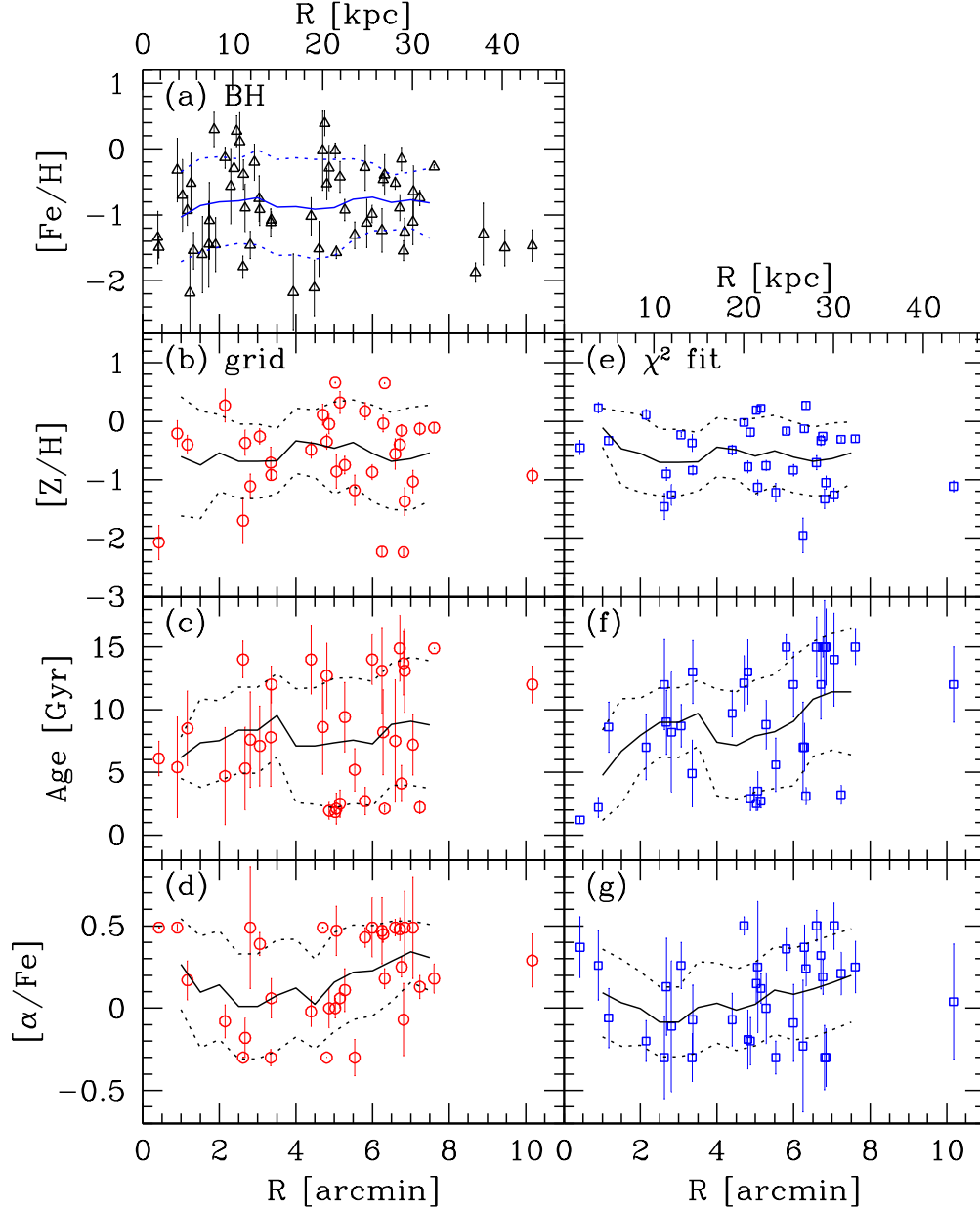


Fig. 6.— Radial variation of metallicity, age, and $[\alpha/\text{Fe}]$: (a) $[\text{Fe}/\text{H}]$ from the BH method, (b) $[\text{Z}/\text{H}]$, (c) Age, and (d) $[\alpha/\text{Fe}]$ from the grid method, and (e) $[\text{Z}/\text{H}]$, (f) Age, and (g) $[\alpha/\text{Fe}]$ from the χ^2 method. The solid and dotted lines represent the mean values and their dispersions derived using a moving radial bin (with 2.5 arcmin width and 0.5 arcmin step).

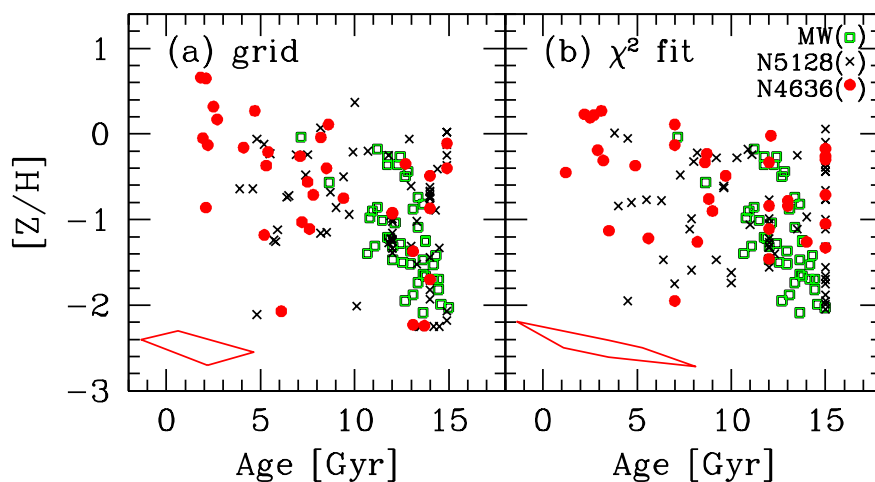


Fig. 7.— Relations between metallicity and age from the grid (a) and the χ^2 minimization method (b). The circles and crosses represent the NGC 4636 GCs in this study and the NGC 5128 GCs derived from indices in Woodley et al. (2010), respectively. The squares represent the MW GCs by Harris (1996) and Carretta et al. (2010). The large boxes represent the mean errors for NGC 4636 GCs.

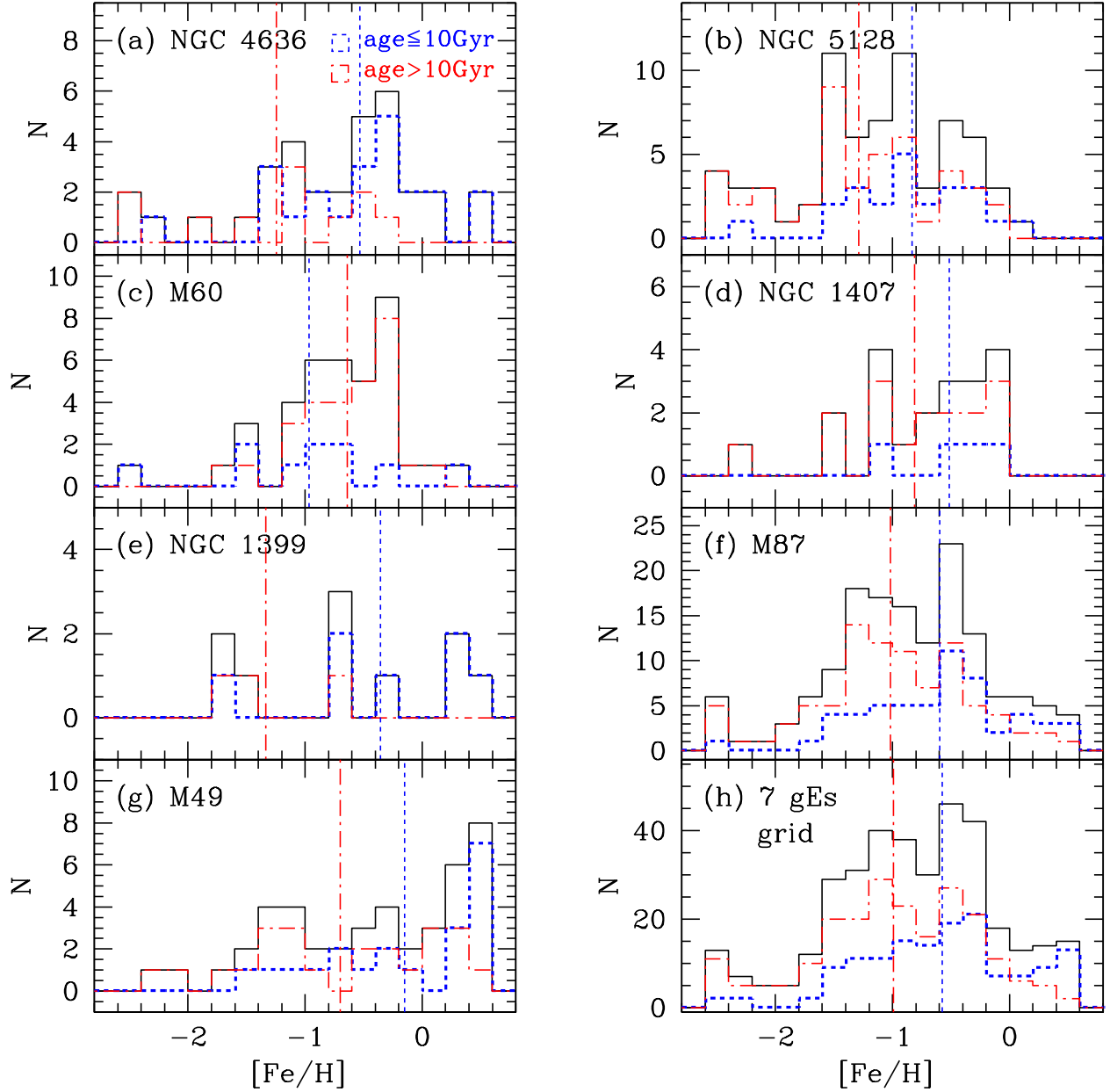


Fig. 8.— Metallicity distribution of GCs in gEs from the grid method. The solid, dot-dashed, and dotted line histograms for gEs show the $[\text{Fe}/\text{H}]$ distributions of all GCs, old GCs (> 10 Gyr), and young GCs (≤ 10 Gyr), respectively. The vertical dotted and dot-dashed lines represent the mean metallicities for young and old GCs, respectively. In panel (h) the histograms represent the metallicity distribution for the combined sample of GCs in all seven gEs.

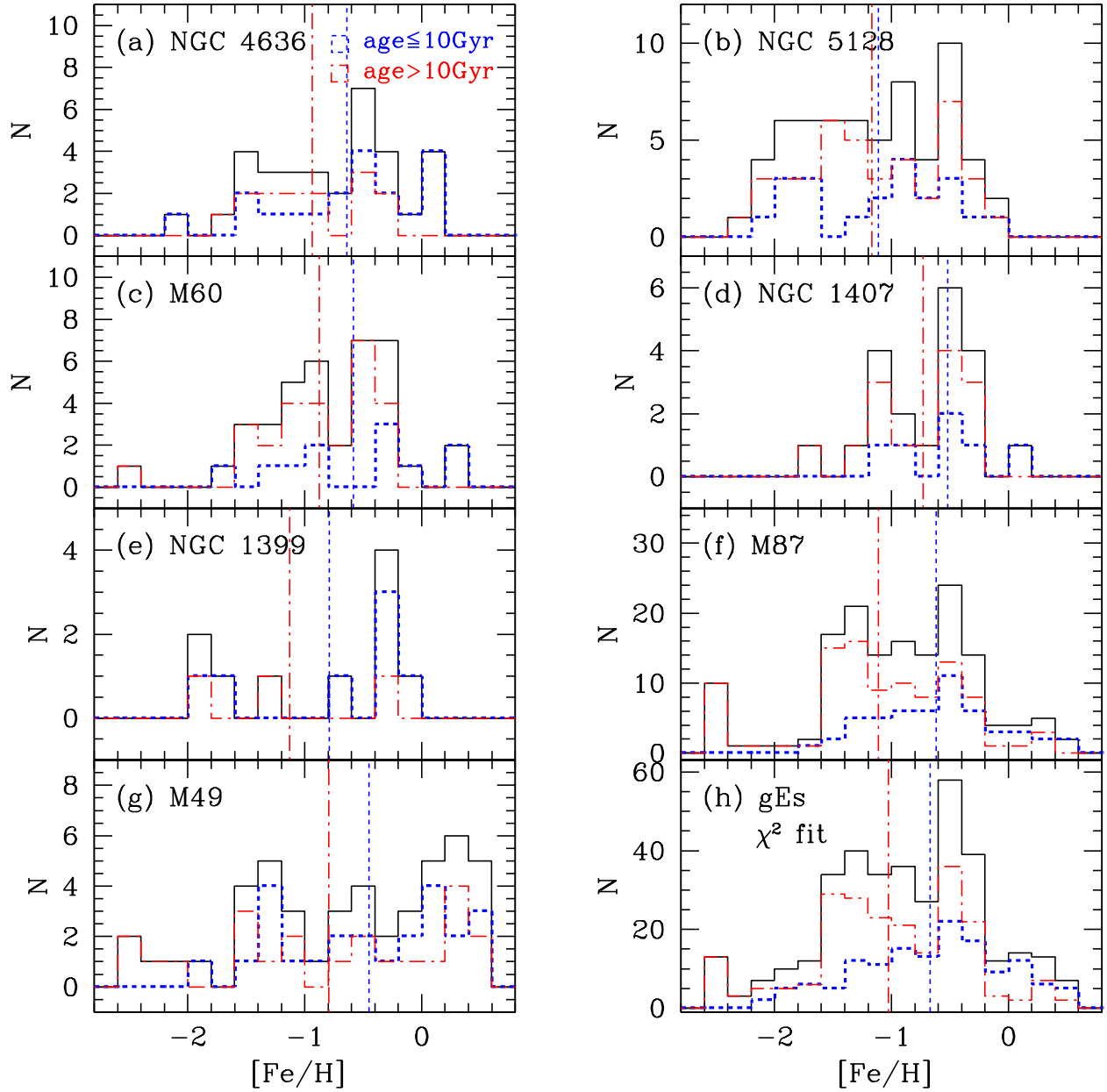


Fig. 9.— Metallicity distribution of GCs in gEs from the χ^2 minimization method. Symbols are same as Figure 8.

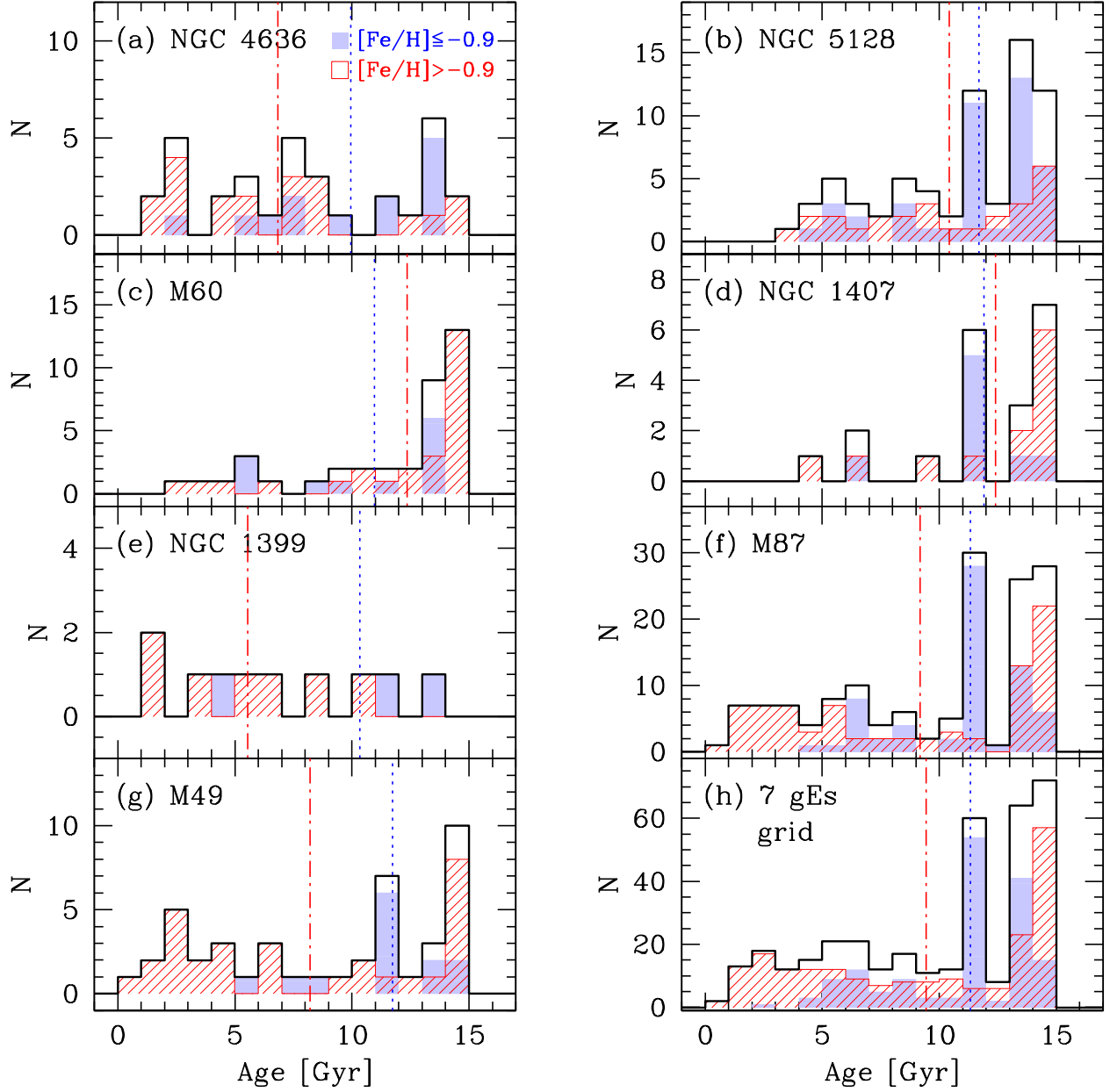


Fig. 10.— Age distribution of the MP ($[\text{Fe}/\text{H}] \leq -0.9$) GCs (shaded histograms) and the MR ($[\text{Fe}/\text{H}] > -0.9$) GCs (hashed histograms) in gEs derived from the grid method. The solid line histograms represent the sum of the MP and MR groups. The mean ages of the MP and MR groups are shown by the dotted and dot-dashed lines, respectively. The histograms on panel (h) show the age distributions for the combined sample of GCs in seven gEs.

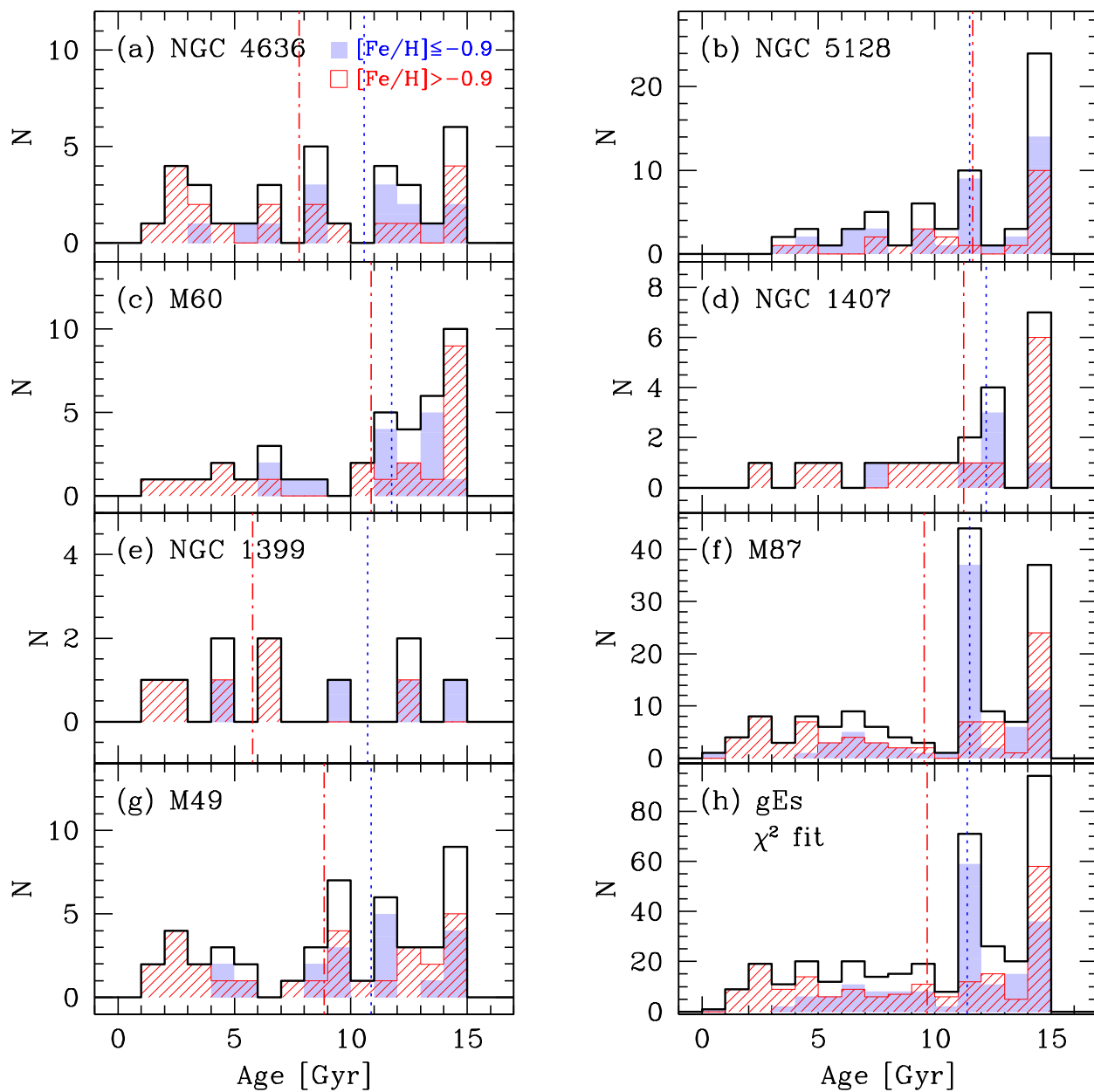


Fig. 11.— Age distribution of GCs in gEs derived from the χ^2 minimization method. Symbols are same as Figure 10.

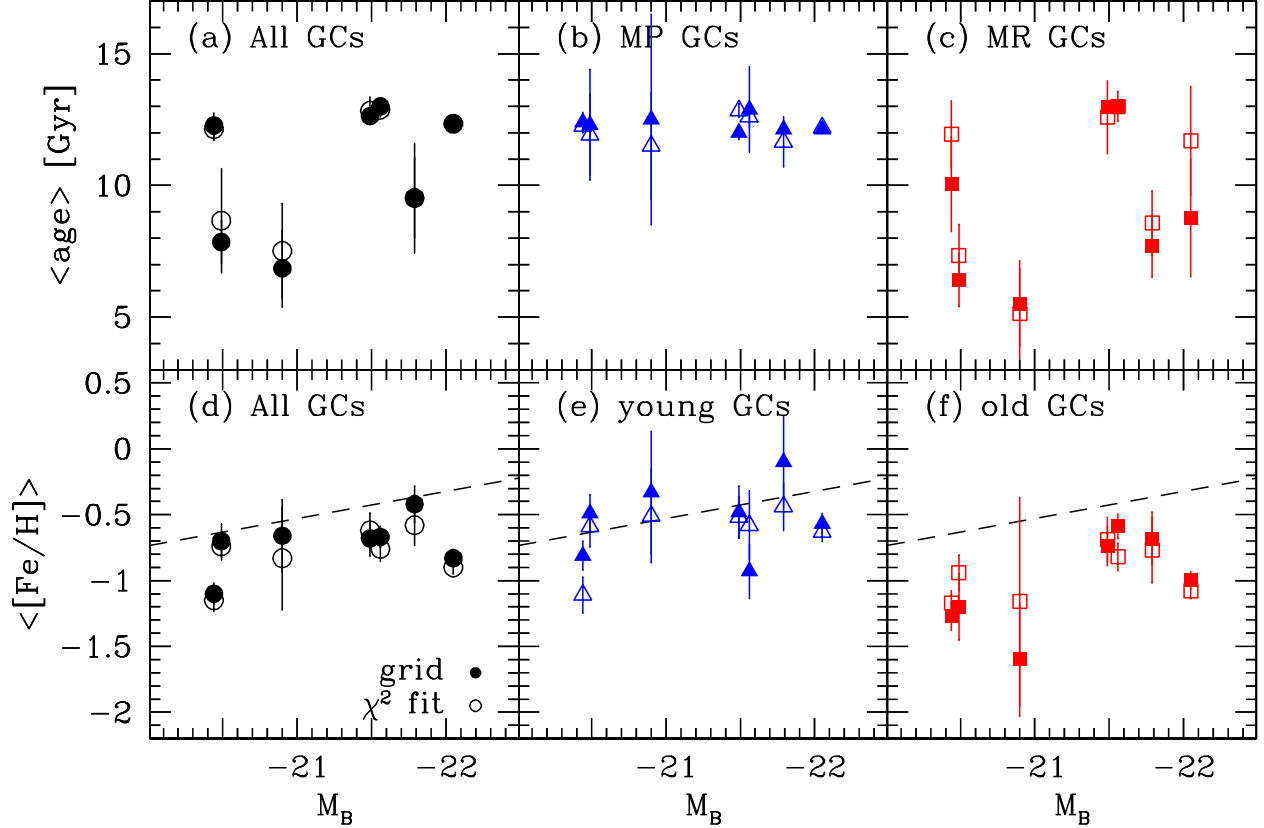


Fig. 12.— Mean ages and metallicities of GCs as a function of absolute magnitude (M_B) of gEs. (a,d) All GCs, (b) MP GCs ($[\text{Fe}/\text{H}] \leq -0.9$), (c) MR GCs ($[\text{Fe}/\text{H}] > -0.9$), (e) young GCs (age ≤ 10 Gyr), and (f) old GCs (age > 10 Gyr). M_B 's of gEs are obtained from HyperLeda (Paturel et al. 2003). The filled and open symbols are from the grid method and the χ^2 minimization method, respectively. The dashed lines represent a relation derived from photometry of GCs in early-type galaxies in Virgo by Peng et al. (2006).

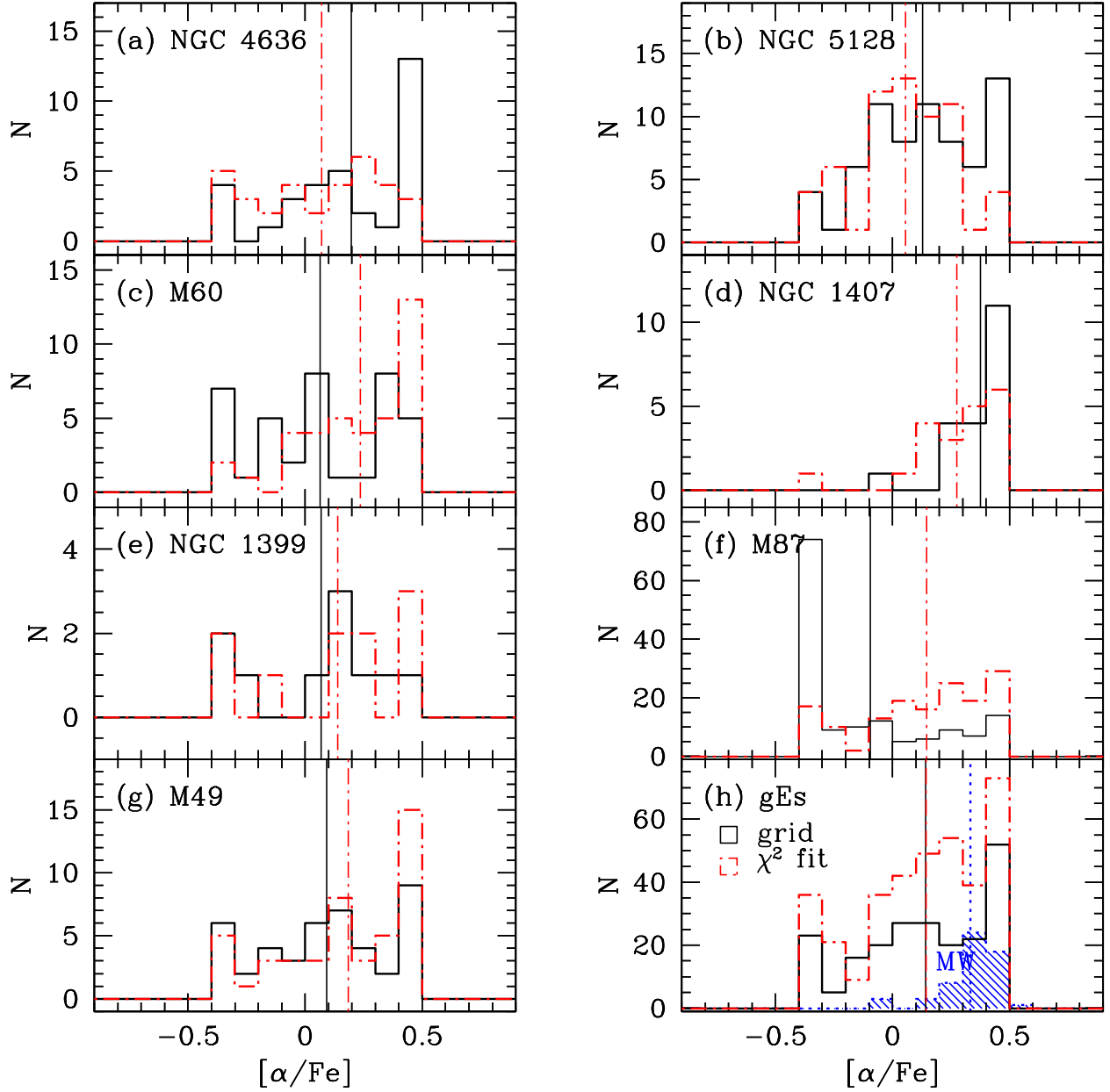


Fig. 13.— $[\alpha/\text{Fe}]$ distribution of GCs in gEs from the grid method (solid) and the χ^2 minimization method (dot-dashed). The vertical lines represent the mean values of the $[\alpha/\text{Fe}]$ of GCs in each galaxy. Panel (h) shows the $[\alpha/\text{Fe}]$ distribution for the combined sample of GCs in six gEs (grid method) excluded M87 GCs and in seven gEs (χ^2 fit). The dotted histogram and line represent the MW GCs.

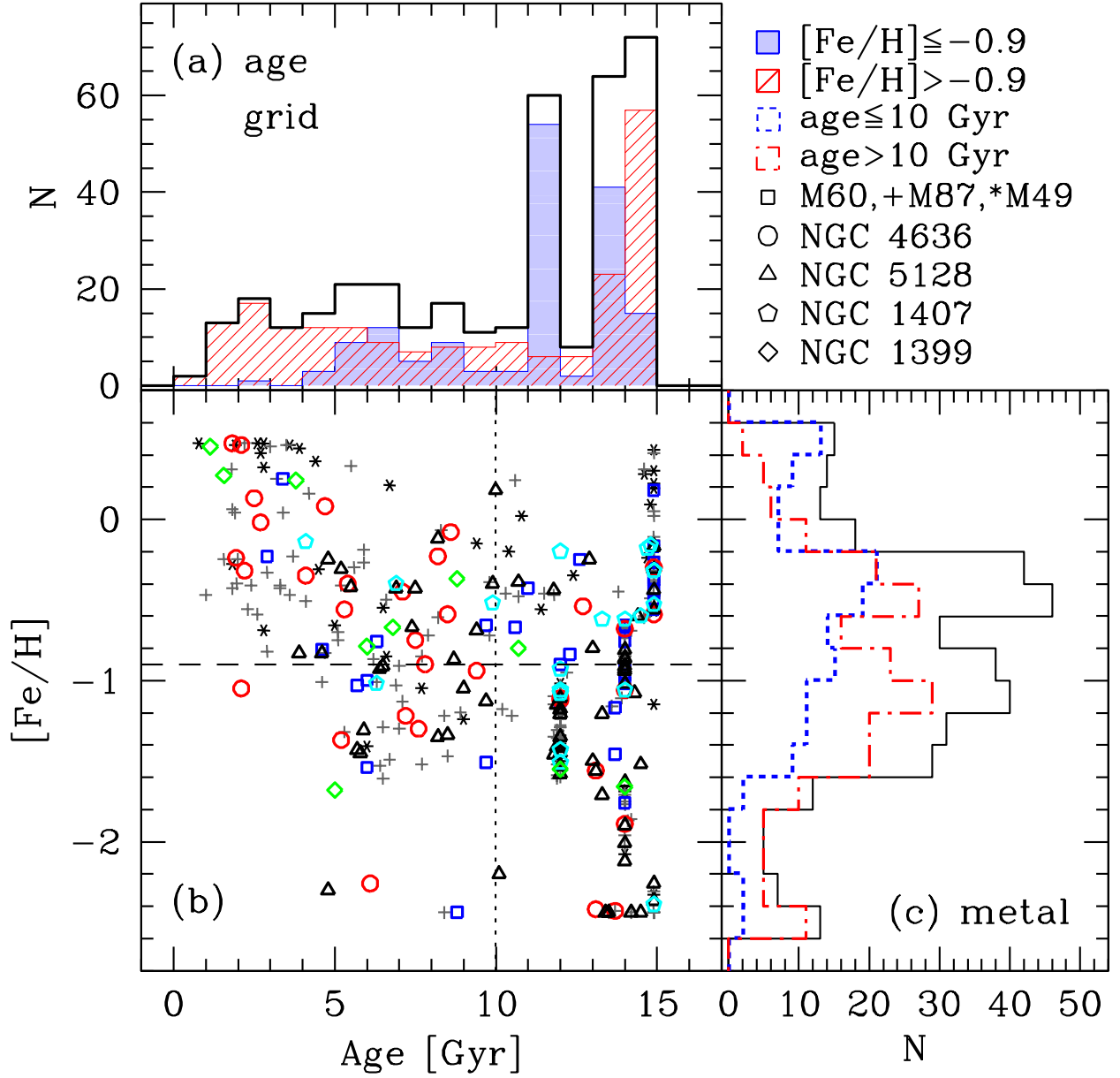


Fig. 14.— Age-metallicity relation of GCs in gEs from the grid method. (a) The solid, shaded, and hashed histograms represent the age distributions of all, MP, and MR GCs, respectively. (c) The dotted and dot-dashed histograms show the $[\text{Fe}/\text{H}]$ distributions for the combined sample of GCs with ages smaller and larger than 10 Gyr, respectively, in seven gEs. The solid histogram represents the metallicity distribution of all GCs. (b) The squares, circles, triangles, pentagons, diamonds, plus, and stars represent the GCs of M60, NGC 4636, NGC 5128, NGC 1407, NGC 1399, M87, and M49, respectively. The vertical dotted line is an age criterion, 10 Gyr, to divide young and old GCs and the horizontal dashed line is a metallicity criterion, $[\text{Fe}/\text{H}] = -0.9$ dex, to divide MP and MR GCs.

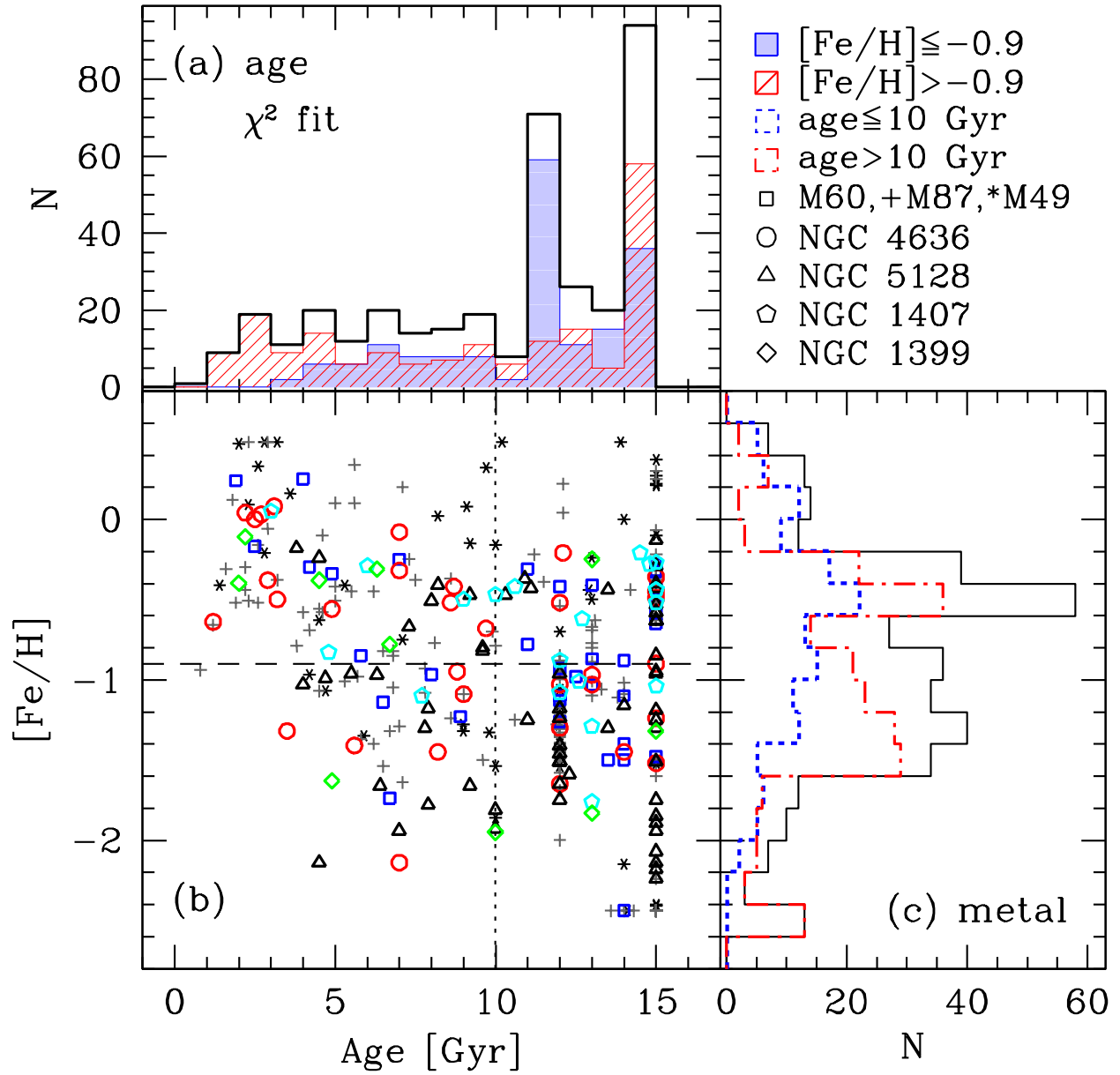


Fig. 15.— Age-metallicity relation of GCs in gEs from the χ^2 minimization method. Symbols are same as Figure 14.